



University of Pennsylvania
ScholarlyCommons


Publicly Accessible Penn Dissertations

2021

Desmin And Microtubules Maintain Nuclear Shape And Chromatin Organization In The Adult Cardiomyocyte

Julie Heffler
University of Pennsylvania

Follow this and additional works at: <https://repository.upenn.edu/edissertations>

 Part of the [Biology Commons](#), and the [Molecular Biology Commons](#)

Recommended Citation

Heffler, Julie, "Desmin And Microtubules Maintain Nuclear Shape And Chromatin Organization In The Adult Cardiomyocyte" (2021). *Publicly Accessible Penn Dissertations*. 4155.
<https://repository.upenn.edu/edissertations/4155>

This paper is posted at ScholarlyCommons. <https://repository.upenn.edu/edissertations/4155>
For more information, please contact repository@pobox.upenn.edu.

Desmin And Microtubules Maintain Nuclear Shape And Chromatin Organization In The Adult Cardiomyocyte

Abstract

Mechanical forces are transduced to nuclear responses via the linkers of the nucleoskeleton and cytoskeleton (LINC) complex, which couples the cytoskeleton to the nuclear lamina and associated chromatin. While disruption of the LINC complex can cause cardiomyopathy, the relevant interactions that bridge the nucleoskeleton to cytoskeleton are poorly understood in the cardiomyocyte, where cytoskeletal organization is divergent from that of other cell types. Furthermore, while microtubules and desmin intermediate filaments associate closely with cardiomyocyte nuclei, the importance of these interactions is unknown. Here, we sought to determine how cytoskeletal interactions with the LINC complex regulate nuclear homeostasis in the cardiomyocyte and health of the myocyte as a whole. To this end, we acutely disrupted the LINC complex, microtubules, actin, and intermediate filaments and assessed the consequences on nuclear morphology and genome organization in rat ventricular cardiomyocytes via a combination of super-resolution imaging, biophysical, and genomic approaches. We find that a balance of dynamic microtubules and desmin intermediate filaments is required to maintain nuclear shape and the fidelity of the nuclear envelope and lamina. Upon depletion of desmin (or nesprin [nuclear envelope spectrin repeat protein]-3, its binding partner in the LINC complex), polymerizing microtubules collapse the nucleus and drive infolding of the nuclear membrane. This results in DNA damage, a loss of genome organization, and broad transcriptional changes. The collapse in nuclear integrity is concomitant with compromised contractile function and may contribute to the pathophysiological changes observed in desmin-related myopathies.

Degree Type

Dissertation

Degree Name

Doctor of Philosophy (PhD)

Graduate Group

Cell & Molecular Biology

First Advisor

Benjamin L. Prosser

Keywords

Cardiac, Cytoskeleton, LINC complex, Mechanobiology, Nucleus

Subject Categories

Biology | Molecular Biology

DESMIN AND MICROTUBULES MAINTAIN NUCEAR SHAPE AND CHROMATIN
ORGANIZATION IN THE ADULT CARDIOMYOCYTE

Julie Heffler

A DISSERTATION

in

Cell and Molecular Biology

Presented to the Faculties of the University of Pennsylvania

in

Partial Fulfillment of the Requirements for the

Degree of Doctor of Philosophy

2021

Supervisor of Dissertation

Benjamin L. Prosser, Ph.D.

Associate Professor of Physiology

Graduate Group Chairperson

Daniel S. Kessler, Ph.D.

Associate Professor of Cell and Developmental Biology

Dissertation Committee

Rajan Jain, M.D., Assistant Professor of Medicine

Paul A. Janmey, Ph.D., Professor of Physiology

Robert L. Mauck, Ph.D., Mary Black Ralston Professor for Education and Research in
Orthopaedic Surgery, Committee Chair

Rebecca G. Wells. M.D., Professor of Medicine

DEDICATION

To the 17-year-old girl who thought making E. Coli fluoresce under UV light was the coolest thing in the world.

ACKNOWLEDGMENT

I want to start this thesis with the deepest gratitude to my advisor Ben for always being my greatest advocate and supporter even when I doubted my work, my motivation, and myself. From the financial and intellectual support through this project to the emotional support when I was unsure that I would ever be successful in this scientific world: truly from the bottom of my heart thank you for being in my corner through the years. I hope when I'm also mentoring students, I also show the same patience and spirit that not only helped keep me sane on difficult days but also kept me motivated and pushing toward creating the best science. Thank you for all the advice and pep-talks through the years. It's really been an honor working and growing with you.

Next, I would like to thank the current and former senior colleagues in the lab that helped train me on my first week in the lab: Pat Robison, Yingxian "Christina" Chen, Matthew Caporizzo, and Alexey Bogush. Similarly, you all showed me unbelievable patience and guidance and showed me how to do all the skills that I am now praised for. Thank you for being the ones on the ground every day showing me how to practically perform good science. Moreover, thanks to all those that came later: Alex Salomon, Keita Uchida, Emily Scarborough, Sai Phyo, Quentin McAfee, JJ Lee and Jennine Dawicki-McKenna. Not only did all the people listed above provide a fun, supportive environment to grow as a scientist, but many of them provided real, hands-on support by doing isolations, helping collect samples, actually running or imaging experiments for me on days when I was too busy or otherwise could not. Of note, Pat, Matthew, Christina,

Alex, Sai, Keita, and Emily all provided data to this body of work, and it would not have been possible without them. The Prosser lab as a whole has truly adopted the “It takes a village to raise a scientist” method of teaching, and I am deeply grateful for all my colleagues for going above and beyond for me through all years.

A special thank you to my collaborators in other Penn labs that have been great sources of intellectual and practical help through this project. Robert Mauck and his lab for early support when we first began looking at alterations to cell stretch and helping us troubleshoot that system. Rajan Jain’s lab (particularly Parisha Shah and Joshua Rhoades) did the overwhelming majority of the work on the lamin B1 ChIPseq and LAD map creation. A particular thanks to Parisha also for the many talks over the years about life and science.

Thank you to my committee members: Drs. Jain, Janmey, Mauck and Wells for their input on my project over the years and support. Many of the questions they asked during our meetings were instrumental in this project’s directions and reality checks for us. Thank you as well to the Cell and Molecular Biology Graduate Group, its leaders and the administrative staff who gave me opportunities to present my work, a place to make friends and life-long colleagues, and the financial and practical support to finish this dissertation.

Lastly, I want to thank my husband Patrick, my parents and all the friends I have made through this experience. It would be an understatement to say the past nearly 6 years of my life have been a rollercoaster. Thanks for riding along. I love you all ♥

ABSTRACT

DESMIN AND MICROTUBULES MAINTAIN NUCEAR SHAPE AND CHROMATIN ORGANIZATION IN THE ADULT CARDIOMYOCYTE

Benjamin L. Prosser, Ph.D.

Mechanical forces are transduced to nuclear responses via the linkers of the nucleoskeleton and cytoskeleton (LINC) complex, which couples the cytoskeleton to the nuclear lamina and associated chromatin. While disruption of the LINC complex can cause cardiomyopathy, the relevant interactions that bridge the nucleoskeleton to cytoskeleton are poorly understood in the cardiomyocyte, where cytoskeletal organization is divergent from that of other cell types. Furthermore, while microtubules and desmin intermediate filaments associate closely with cardiomyocyte nuclei, the importance of these interactions is unknown. Here, we sought to determine how cytoskeletal interactions with the LINC complex regulate nuclear homeostasis in the cardiomyocyte and health of the myocyte as a whole.

To this end, we acutely disrupted the LINC complex, microtubules, actin, and intermediate filaments and assessed the consequences on nuclear morphology and genome organization in rat ventricular cardiomyocytes via a combination of super-resolution imaging, biophysical, and genomic approaches. We find that a balance of dynamic microtubules and desmin intermediate filaments is required to maintain nuclear shape and the fidelity of the nuclear envelope and lamina. Upon depletion of desmin (or nesprin [nuclear envelope spectrin repeat protein]-3, its binding partner in the LINC complex), polymerizing microtubules collapse the nucleus and drive infolding of the nuclear membrane. This results in DNA

damage, a loss of genome organization, and broad transcriptional changes. The collapse in nuclear integrity is concomitant with compromised contractile function and may contribute to the pathophysiological changes observed in desmin-related myopathies.

TABLE OF CONTENTS

DEDICATION.....	ii
ACKNOWLEDGMENT.....	iii
ABSTRACT.....	v
LIST OF ILLUSTRATIONS.....	ix
CHAPTER 1: INTRODUCTION AND METHODS.....	1
Introduction.....	1
Methods.....	8
Animals.....	8
Adult myocyte isolation and culturing.....	8
Neonatal myocyte isolation and culturing.....	9
Pharmaceuticals.....	10
Virus generation and vectors.....	10
RT-qPCR.....	11
Western blot.....	12
Histone extraction.....	12
Immunofluorescence.....	13
Imaging equipment and analysis.....	14
Microtubule imaging acquisition and analysis.....	15
Nuclear dimension measurements.....	16
Measurements of calcium transients and contractility.....	16
ChiP-seq.....	18
Electron microscopy.....	20
Whole animal studies.....	21
Statistics.....	22
CHAPTER 2: DESMIN AND MICROTUBULES MAINTAIN NUCLEAR STRUCTURE AND GENOME ORGANIZATION.....	23

Modulation of the cytoskeleton alters nuclear morphology.....	23
Acute desmin depletion causes nuclear infolding and chromatin compaction.....	25
Depletion of nesp-3 phenocopies the nuclear involution seen upon desmin depletion....	26
Nuclear infolding is driven by dynamic microtubules.....	27
Desmin depletion leads to DNA damage.....	30
DN-KASH causes DNA damage.....	31
Desmin depletion disrupts nuclear homeostasis <i>in vivo</i> and <i>in situ</i>	32
Acute reduction in desmin via dTAG degron causes nuclear involution in mice.....	34
CHAPTER 3: FUNCTIONAL CONSEQUENCES OF ACUTE DESMIN DEPLETION.....	36
Desmin depletion drives large-scale changes to gene expression and compromises lamina-associated chromatin.....	36
Acute desmin depletion disrupts excitation-contraction coupling.....	38
Acute desmin depletion alters cellular stiffness and microtubule buckling.....	39
CHAPTER 4: CONCLUSIONS AND FUTURE DIRECTIONS.....	41
BIBLIOGRAPHY.....	47
ILLUSTRATIONS.....	61

LIST OF ILLUSTRATIONS

Graphical Abstract: Desmin and microtubules work in concert to maintain nuclear homeostasis and chromatin organization.....	61
Figure 1: Acute desmin depletion causes involution of cardiomyocyte nuclei.....	62
Supplemental Figure 1: Desmin knockdown does not affect cell size.....	64
Figure 2: Acute desmin or nesprin (nuclear envelope spectrin repeat protein)-3 depletion causes lamina infolding.....	65
Supplemental Figure 2: Multiple nesp-3 shRNA variants are able decrease nesprin-3 levels...	67
Supplemental Figure 3: Multiple nesprin-3 shRNA variants cause nuclear infolding in a microtubule-dependent manner.....	69
Figure 3: Disrupting dynamic microtubules prevents nuclear defects arising from desmin or nesprin (nuclear envelope spectrin repeat protein)-3 depletion.....	71
Supplemental Figure 4: Nuclear infolding is irreversible but is not associated with changes to Lamin A/B1/C levels.....	73
Supplemental Figure 5: DN-KASH causes nuclear swelling, rescues desmin and nesp-3 KD...	75
Figure 4: Desmin knockdown (KD) causes DNA damage that is partially prevented by microtubule depolymerization.....	77
Figure 5: DN KASH causes elevated γ H2AX in adult rat cardiomyocytes.....	79
Figure 6: Desmin knockdown (KD) causes nuclear malformation in vivo.....	80
Figure 7: Desmin protects from microtubule-dependent nuclear disruption in beating cardiac syncytia.....	82
Figure 8: dTAG Desmin degron system causes efficient desmin degradation and nuclear abnormalities.....	84
Figure 9: Desmin knockdown (KD) results in large-scale changes to gene expression and compromises lamina-bound chromatin.....	86
Supplemental Figure 6: Lamin-B1 ChIP immunoprecipitation (IP) and sequencing are both functional.....	88

Figure 10: Excitation-contraction coupling is similarly altered upon acute desmin or nesprin (nuclear envelope spectrin repeat protein)-3 depletion.....89

Figure 11: Figure 11: Desmin KD decreases the viscoelasticity of adult cardiomyocytes.....90

Figure 12: Desmin KD causes microtubules to contract with longer wavelengths.....91

Figure 13: Desmin KD reduces tyrosinated microtubules.....92

CHAPTER 1: INTRODUCTION AND METHODS

Portions adapted from (78): Heffler, J., Shah, PP., Robison, P., Phyo, S., Veliz, K., Uchida, K., Bogush, A., Rhoades, J., Jain, R. and Prosser, BL. A Balance Between Intermediate Filaments and Microtubules Maintains Nuclear Architecture in the Cardiomyocyte. Circulation Research. 2019;126:e10-e26. doi: 10.1161/CIRCRESAHA.119.315582Ci

Cardiac myocytes generate the contractile force required to pump blood throughout the body. They experience cyclic stress and strain with each heartbeat, and alterations in these mechanical stressors can lead to cardiomyocyte hypertrophy and eventually heart failure.

Over the past century, it has become more well-appreciated that there is a link between changes to the mechanical environment in the heart, pathological remodeling on both the cellular and tissue level, and eventual heart disease and failure. Moreover, those remodeling changes themselves can serve as a feedback loop to further exacerbate pathological strain on the myocardium. For example, increased pressure that the heart has to pump against (pressure overload) induces cardiomyocytes to undergo concentric hypertrophy (parallel sarcomere growth or preferential growth in width). This, in addition to changes to the extracellular matrix such as increased fibrosis due to decreased collagen degradation by cardiac fibroblasts (1), is associated with thickening and stiffening of the heart walls. Conversely, an increase in cellular stretch is associated with

volume overload. This tends to cause eccentric hypertrophy (in series sarcomere growth or preferential growth in length) and thinning of the heart walls (2).

While several force-dependent signaling cascades that regulate cardiomyocyte growth have been described (3), our understanding of how mechanical forces are sensed and transduced is still underdeveloped. Many different pathways need be considered when attempting to categorize how mechanical signals are translated into changes to gene transcription and eventually to overall heart health and disease. These include but aren't limited to: 1) kinase modulation via integrin complexes, costameres, and cell-to-cell junctions such as through focal adhesion kinase (FAK) 2) membrane-tension inducing conformational changes to mechanosensitive ion channels (ex: TREK1) 3) tension on cytoskeletal elements that then in turns modulates actin-, microtubule- and intermediate filament-associated kinase signaling pathways or ion channels (ex: TRPV4 and Piezo channels) and 4) tension transmission to the nucleus that directly modulates both lamin-bound chromatin and signaling proteins attached to the lamina and 5) regulation of miRNA via mechanical tension to the nucleus (4-5).

The nucleus is thought to be a key integration site for many of signals whether via the aforementioned indirect activation of genes via kinase signaling pathways or directly by its physical connection to the cytoskeleton. Recent work, primarily conducted in non-muscle cells, has demonstrated that, alongside force-dependent signaling cascades, mechanical forces can also be transmitted directly to the nucleus via the Linkers of the Nucleo- and Cytoskeleton (LINC) complex to modulate force-dependent gene expression. The LINC complex is

composed of the nuclear envelope spectrin repeat proteins (nesprins) 1-4 in the outer nuclear membrane and the Sad1p-UNC-84 (SUN) domain 1 and 2 proteins in the inner nuclear membrane. This complex anchors actin filaments, microtubules, and intermediate filaments to the nucleus. SUN proteins link to the nuclear lamina, which in turn directly binds chromatin in lamina-associated chromatin domains (LADs). Hence, the LINC complex forms a contiguous route for force transmission from the cytoskeleton to chromatin (4, 6).

The nesprin proteins come not only in 4 genes but are also variably spliced, with nesprin-1 having at least 5 splice forms, nesprin-2 with at least 6, and nesprin-3 with 2. For the purposes of this thesis, we will focus only on nesprins-1-3 as nesprin-4 is not expressed in the heart for rodents. For nesprin-1 and nesprin-2, only their unspliced, “giant” forms (“nesprin-1G” and “nesprin-2G” respectively) contain a calponin homology (CH) domain near the N-terminus, allowing it to bind to actin (7). Moreover, both nesprin-1 and -2 have been thought to associate with both kinesin and dynein to microtubules via domains closer to their C-terminus (8-9), allowing for many different interactions with these variably spliced proteins. Lastly, nesprin-3 α has been shown to be the splice form of nesprin-3 that interacts with plectin and intermediate filaments. The purpose of nesprin-3 β remains unclear (10-11).

The SUN proteins, in contrast, exist in two isoforms (SUN1 and 2) and have had more study in their involvement in meiosis and the DNA damage response. SUNs are necessary for homologous recombination during meiosis and for repairs to double-stranded breaks. The LINC complex has also been associated

with its involvement in maintaining lamina and nuclear integrity by preventing weakening of the lamina and subsequent rupture (5,12). However, much of this work has been conducted in non-striated muscle. Thus, the precise cytoskeletal connections to the nucleus that are relevant to cardiomyocyte biology remain largely mysterious. This area of study is of clinical importance, as mutations in many cytoskeletal, LINC complex, and lamin proteins are associated with cardiomyopathy (13-15), and rodent studies demonstrate that loss of LINC proteins is sufficient to cause cardiomyopathy (16).

This becomes a key area of study and question as the cytoskeleton of the adult cardiomyocyte is highly divergent of that from other cells in the body. The actin and myosin networks are organized into complex structures known as sarcomeres which provide the contractile force necessary to shorten the myocyte upon electrical stimulation. These sarcomeres are organized into myofilaments, connected to one another longitudinally via the z-disc which is composed of not only several structure components such as α -actinin and desmin but many mechanotransductive elements such as muscle LIM protein (MLP), calsarcin-1 and melusin (17). Laterally, these myofilaments are coupled to one another via desmin and other intermediate filaments to create a highly coordinated and interconnected contractile machine. Moreover, these myofilaments are also physically coupled via microtubules, non-sarcomeric actin and intermediate filaments to the cell periphery and the surrounding extra cellular matrix (via costameres) and to different organelles (such as the nucleus and the mitochondria) (10-11, 18-20). Of note, alterations in the localization, post-

translational modulation, expression, and degradation of the actomyosin, microtubule and intermediate filament are highly associated with heart health and disease. For example, desmin and detyrosinated microtubules are highly elevated in heart failure leading to a more viscous and stiffened myocardium while contractile machinery is down regulated (21).

Desmin, the aforementioned coupler of myofilaments at the z-disc, is a type-III muscle-specific intermediate filament and is the predominant intermediate filament in muscle. Desmin forms a honeycomb-like scaffold that wraps around the sarcomere at the z-disc, coupling it to the sarcolemma, intercalated disk and various organelles including the mitochondria and the nucleus (22). Desmin is involved in transmitting strain through muscle (23), for the proper maintenance of mitochondrial morphology and function (18-20), and recent work suggests desmin may function as a signaling platform for mechanosensing (24). Mutations in desmin or desmin chaperones lead to “desminopathies,” (13, 25) a broad spectrum of muscle diseases that include myofibrillar myopathy, arrhythmogenic cardiomyopathy, and dilated cardiomyopathy (14), and both loss (26) and gain (27-29) of desmin function are sufficient to induce heart disease. With respect to its interactions with the nucleus, desmin remains understudied. As previously mentioned, desmin has been shown to be in close proximity to the nuclear envelope and to co-immunoprecipitated with plectin and nesprin-3 (10-11), but the importance of this interaction is unknown.

Another important cytoskeletal connector, microtubules, has received much attention in the past 10 years on its role in regulating cardiomyocyte health. The

microtubule network runs primarily longitudinally down the length of the cardiomyocyte, nucleating from organizing centers peripheral to the nucleus. They serve as structural elements that buckle and bear load during cardiomyocyte contraction, (30), transportation networks for vesicles and mRNA (31), and are an important tension sensory network (32-33). The organization of this network is also hypothesized to be partially regulated by its interaction with desmin, the loss of which causes the network to become more vertically oriented and scattered (30).

As both these cytoskeletal networks (desmin and microtubules) are critically important for a variety of homeostatic and sensory functions in the cell and are both physically coupled with the nucleus via the LINC complex, we sought to further the field's understanding of their purpose in the adult cardiomyocyte with regard to nuclear homeostasis. Here we sought to determine how desmin, microtubules, and actin maintain nuclear morphology in this system. We utilized genetic and pharmacological tools to disrupt cytoskeletal interactions with the nucleus and interrogated structural and functional consequences using a combination of high-resolution microscopy, transcriptomic and genomic assays, and functional tests.

Firstly, we found that desmin is required to maintain nuclear shape in a microtubule-dependent manner. Without desmin or its LINC binding partner nesprin-3, cardiomyocyte nuclei begin to shrink and deform, developing deep invaginations that go into the center of the nucleus. These folds are dependent on the presence of polymerizing microtubules and presumed to act through

nesprin-1/2. Moreover, we found that loss of desmin causes loss of chromatin organization particularly the attachments to the nuclear lamina. This loss of lamina associated domains (LADs) is associated with large-scale changes to the transcriptome with a third of detected transcripts having a significant change in level. These changes are also associated with loss of cardiomyocyte contractility.

Secondly, we observed changes to the microtubule network with the loss of desmin. As mentioned previously, desmin is hypothesized to be an important anchor of microtubules to the z-disc and keep the microtubule network organized and reinforced. In the absence of desmin, there is a loss of both tyrosinated and detyrosinated microtubules. Moreover, the stereotyped buckling that occurs at the z-disc is lost and microtubules buckle at much longer wavelengths, inefficiently dispersing strain. Together these data imply a feedback loop between desmin and microtubule organization to not only maintain nuclear homeostasis but the organization of the whole cytoskeletal network.

Lastly, we were able to replicate many of these findings in cultured pseudo-tissues and *in vivo*. We were able to show that even in neonatal rat ventricular myocytes and in mature, adult cardiac tissue, acute loss of desmin causes malformations in the nuclear lamina. In cultured cardiac syncytia, we were able to replicate the increase in the DNA-damage response and the dependency on polymerizing microtubules. Moreover, we were able to show in a non-viral-mediated system that acute degradation of desmin protein causes similar phenotypes (nuclear malformation and lamina folding) to those we observe with adenoviral-mediated knockdown.

Taken as a whole, these data reinforce the integral nature of the non-sarcomeric cytoskeleton to the health and function of the adult cardiomyocyte, and further suggest a push-pull balance between microtubules and intermediate filaments that preserves nuclear homeostasis and cardiomyocyte function.

METHODS

Animals: Animal care and procedures were approved and performed in accordance with the standards set forth by the University of Pennsylvania Institutional Animal Care and Use Committee and the Guide for the Care and Use of Laboratory Animals published by the US National Institutes of Health. Inclusion criteria for this study for all but the neonatal studies required that the rats were adult (>8 weeks of age) male Sprague Dawley rats. Rats were excluded if they showed any sign of illness.

Adult myocyte isolation and culturing: Primary adult ventricular myocytes were isolated from 8- to 12-week-old Sprague Dawley rats using Langendorff retrograde aortic perfusion with an enzymatic solution. Cardiomyocytes were then cultured for 24 to 72 hours depending on the experimental paradigm. For details of cardiomyocyte isolation and culture please see reference (30). A subset of cardiomyocytes were labeled with calcein-AM (Thermo Fisher Scientific C1430) and attached to Nunc 8 well chambered cover glasses (Thermo Fisher Scientific 155409PK) to track the morphology of individual cardiomyocytes with

viral transduction over 72 hours in culture. Cells were excluded from study if they were clearly dead, malformed/hypercontracted or displayed loss of membrane integrity.

Neonatal myocyte isolation and culturing: Neonatal rat ventricular myocytes (NRVMs) were isolated from P1-P2 mice. Pups were anesthetized on ice, rapidly decapitated and their hearts were exercised and placed in chilled Hank's Balanced Salt Solution (HBSS, Sigma 21-021-CM). Pooled hearts from a single litter were minced and digested in HBSS containing trypsin (Worthington LS003703) and benzonase (Sigma E1014-5KU). Cells were gently centrifuged, resuspended in serum-containing NRVM media (DMEM (Gibco 11965-084), 5% FBS, 12.5 mM HEPES (University of Pennsylvania Cell Center, 1M stock), 4 mM Aln-Gln (Sigma G8541-100ml) and 0.1 mg/ml primocin (InVivoGen ant-pm-1, 50 mg/ml stock)) and pre-plated for 2 hours to remove a large portion of the cardiac fibroblast pool. Cells were counted and plated at 100-300,000 cells/cm (Bish Human Gene Therapy 2008).

NRVMs were cultured primarily on nano-patterned surfaces to aid in their maturation and alignment (NanoSurface Biomedical glass coverslips (ANFS-CS12), glass-bottom dishes (ANFS-0001) or PDMS Cytostretch Chamber (CS-01444-PPA)). These surfaces were coated with collagen to promote adhesion. Coating was performed by plasma cleaning surfaces followed by immediate incubation with 0.01% collagen (Sigma C8919-20ml, 0.1% stock in acetic acid) in PBS (Quality Biological 119-069-131) at 37 C overnight. Cells were allowed to

adhere to surfaces following pre-plating for 24-48 hrs post isolation and then switched to serum-free media (DMEM (Gibco 11965-084), 1% ITS (Gibco 51500-056), 12.5 mM HEPES (University of Pennsylvania Cell Center, 1M stock), 4 mM Aln-Gln (Sigma G8541-100ml), 0.1 mg/ml primocin (InVivoGen ant-pm-1, 50 mg/ml stock), 1 mg/ml BSA (Sigma A7906-100G)) where they were kept for 48-72 hrs to synchronize the cell cycle, followed by treatments with either viruses (see below) or Lipofectamine 3000 (Invitrogen L3000-001).

Pharmaceuticals: Colchicine (1 or 10 μ M in DMSO, Sigma C9754), Latrunculin A (10 μ M in DMSO, abcam ab144290), Y27632 (10 μ M in DMSO, Sigma Y0503-1MG), Y16 (Sigma SML0873-5MG), Nocodazole (0.5 μ M Fisher Scientific AC358240100), and Taxol (10 μ M).

Virus generation and vectors:

Desmin KD Adenovirus (AdV): Desmin KD AdV (AdV-U6-GTCCTACACCTGCGAGATTG-76K-AAGCAGGAGATGATGGAAT-EF1a-eBFP2) was generated and produced as previously described for the dual promotor (U6 and 76K) shTTL construct (30) with target shRNA sites listed above. eBFP2 was used as a transduction marker instead of mCherry.

Desmin KD Adeno-associated virus: Plasmid used to generate desmin KD AdV with the same dual-promotor set-up was sent to the University of Pennsylvania's vector core (pennvectorcore.med.upenn.edu) to generate AAV9-U6-

GTCCTACACCTGCGAGATTG-76K-AAGCAGGAGATGATGGAAT-EF1a-

eBFP2, using viral production methods previously described (Bish Human Gene Therapy 2008).

LaminB1-mCherry AdV: Mouse LaminB1 with C-terminal fused mCherry AdV was generated and produced using the same Gateway (ThermoFisher) system as described previously (30).

Nesprin-3 KD AdV: nesprin-3 KD AdV was generated in a similar manner as above but directed toward single target sites under the U6 promotor in two separate viruses var1: GCTCCATCCTACAGACAAACA var2: GCTGCACAATGTGGACAATCA var3: GCCTGCTTGTTTCAGCACAAGG. These sites were chosen as they are present in all splice forms of nesprin-3, but absent in nesprin-1 and nesprin-2. eBFP2 was used as a transduction marker.

RT-qPCR: RNA was isolated from adult cardiomyocytes 48-hours post infection using RNAzol (Molecular Research Center RN190) following manufacturer's protocol. cDNA was generated using synthesis kit (Takara Bio 6110A) and included protocol. Following cDNA synthesis, qPCR was performed using master mix (Integrated DNA Technologies 1055770) and primers nesprin-3 (Thermo Rn01518288_m1 SYNE3 FAM which detects the boundary between exons 17 and 18 of Nesp-3 mRNA. This region is conserved in both Nesp-3 and Nesp-3 splice forms and will detect both mRNAs.) and GAPDH (Thermo Rn01749022_g1 VIC) in biological triplicate and technical duplicate. Fold change (FC) was determined via $2^{(-\Delta\Delta CT)}$ equation.

Western blot: Western blot was performed as described previously (30). The western blots in the supplement and with nesprin-3 were generated with a modified protocol whereby the western was developed with ECL instead of infrared-conjugated secondary antibodies. Nesprin-3 blotting was performed using 1:500 nesprin-3 antibody (abcam ab186751) overnight at 4 C in 5% milk in TBST. Antibody specificity was confirmed via knockdown of the specific proteins of interest and secondary only controls.

Histone extraction: γ H2AX western was performed on samples subjected to histone extraction to improve the signal to noise ratio of histone signals (Garcia Proteome Res 2008). Nuclear fraction enrichment was performed (NE-PER Nuclear and Cytoplasmic Extraction Thermo 78833) as per ThermoFisher protocol until cytoplasmic and nuclear extracts were separated. To extract histones, ~400 L of 0.4N/0.2M H₂SO₄ was added slowly to nuclear extracts while vortexing, to a final ratio of 5:1. Nuclei were then resuspended and incubated overnight on a rocking platform in the cold room. This suspension was then centrifuged at 21000xg and the supernatant was moved to a new tube. To this supernatant, chilled, 100 percent trichloroacetic acid was added at 25 percent supernatant volume, incubated for 1 hour on ice and centrifuged at 10000xg. The supernatant was then discarded, and the histone pellet was washed in 1 mL chilled acetone with 0.1 percent HCL without disturbing the pellet, before again centrifuging at 10000xg and discarding the supernatant. The

pellet was then washed in chilled 100 percent acetone, again without disturbing the pellet. The pellet was then air dried for 10 minutes at room temperature, resuspended in water, and incubated for 15 minutes at room temperature before centrifuging once more using a mini benchtop centrifuge for 1 minute. The supernatant was then blotted for histones and γ H2AX.

Immunofluorescence: All cells were fixed in pre-chilled 100% methanol for 8 minutes at -20 C. Cells were washed 4x and blocked with Sea Block Blocking Buffer (abcam166951) for at least 1 hour followed by incubation with antibodies in the same buffer for 24-48 hours (see table below). Primary incubation was followed by washing 3x with Sea Block, and then incubation with appropriate secondaries (see table below) for 1 hour. Lastly, samples were incubated with Hoechst (1:1000 Sigma B2261-100MG) for 10 minutes then washed 4x in PBS (Quality Biological 119-069-131) and mounted using Prolong Diamond (Thermo P36961).

Primary antibodies: Lamin A/C (1:1000 Abcam ab8984), Lamin B1 (1:1000 Santa Cruz sc-374015 or Abcam ab16048), Desmin (1:500 Invitrogen PA5-16705), Nesprin-1 (1:250 Abcam ab192234), Nesprin-2 and Nesprin-3 (Kindly provided by Gant Luxton), Alpha -Tubulin (1:250 Cell Signaling 3873S). Primary antibodies were validated either via previously described staining patterns or via disruptive agents (ex: knockdown of protein, destabilizing drugs, etc), as well as secondary-only controls.

Secondary antibodies: Goat anti-mouse AF 488 (1:1000 Life Technologies A11001), Goat anti-rabbit AF 565 (1:1000 Life Technologies A11011). Secondary antibodies were validated by secondary-only staining.

For directly conjugated antibodies, Lightning Link Rapid Atto565 (Innova Biosciences, 351-0030), Atto 488 (322-0010), and dylight 488 (350-0010) were used to create the direct conjugation.

Imaging equipment and analysis: Confocal imaging was carried out on a Zeiss 880 Airyscan confocal microscope operating on an Axiovert Z1 inverted microscope equipped with EC Plan-Neofluar 10x air 0.30 numerical aperture (NA), Plan-Apochromat 20x air 0.8 NA, Plan-Apochromat 40x oil 1.4 NA, C-Apochromat 40x water 1.2 NA, and Plan-Apochromat 63x oil 1.4 NA objectives. Calcium and contractility measurements were performed on an Axiovert Z1 inverted microscope using C-Apochromat 40x water 1.2 NA objectives. Image analysis was performed using ZEN Black software for Airyscan processing, which involves signal integration from the 32 separate sub-resolution detectors in the Airyscan detector and subsequent deconvolution of this integrated signal. Image processing was performed using FIJI.

Structure illuminated microscopy (SIM) was performed as previously described (21).

Microtubule imaging acquisition and analysis

Buckling: Adult rat cardiomyocytes were isolated as previously described and infected with adenovirus carrying the microtubule-binding protein EMTB chimerically fused to 3 copies of GFP. The purpose of this construct was to label microtubules fluorescently for imaging. The cells were allowed 48 hours to express the construct. All cells chosen were those that contained sufficient brightness and contrast to observe microtubule elements and where the health of the myocyte was not compromised. To interrogate microtubule buckling amplitude and wavelength, cells were induced to contract at 1 Hz 25 V and imaged during the contraction. For analysis, a microtubule was located that could be followed during the contraction. The backbone was manually traced at rest and during its peak of contraction and the ROI was saved. The ROI was then analyzed using a macro that rotated so that the ROI had the peak of contraction 90 degrees to the axis of contraction to protect from aliasing errors. The program then calculated the distance between the axis of the ROI and its peak and calculated the peak (amplitude) and the width (half wavelength).

Immunofluorescence coverage analysis: Cells were fixed and stained as described above. We used an ImageJ to determine the fractional area coverage of desmin and microtubules in in the region of the cardiomyocyte within the boundary of the cell excluding the nucleus. Briefly, an ImageJ macro was written to allow for the automated calculation of tyrosinated, detyrosinated and desmin coverage from immunofluorescence images of the cardiomyocyte and the union

of the detyrosinated and tyrosinated masks were used to determine the total tubulin coverage.

Nuclear dimension measurements: Nuclear dimensions were taken on live cardiomyocytes stained with Hoechst (10 ug/ml for 5 min) or DRAQ5 (5 μ M for 5 min). For manual measurements (Fig 1 and 4), length, width and height were pulled based on an approximation of the long and short axes of an ellipse (i.e., fit through the center of the nucleus rather than the longest measurements). Length is defined as the axis parallel to the contractile/long axis of the cell. Width is defined as the short axis in the xy plane of the cell (transverse axis) perpendicular to length. Height is defined as the short axis in z, which is measured from confocal z-sections and measurement of the zy or zx plane. Volume was determined by a fit to an ellipsoid. Later, 2D measurements were performed via automated particle analysis (Fig 3 and 6). In brief, automated detection was done in FIJI whereby cells loaded with Hoechst or DRAQ5 were imaged at 20x magnification with both 2.5 μ m z-step and tile-scan, taking a bird's eye view of the field of cells. Image was subjected to a median filter (2 pixel), manual thresholding of the nuclear signal, and automated particle analysis to determine size parameters. Nuclei from dead cells were excluded.

Measurements of calcium transients and contractility: Adult cardiomyocytes were loaded with the calcium-sensitive dye Fluo-3-AM (1 μ M) and electrically stimulated at 1 Hz to simultaneously measure changes in the intracellular calcium transient

and the degree of cell shortening, as described previously using Ionoptix equipment with small changes (30). Here, cells were illuminated with broad wavelength light via an X-Cite 120 PC Lamp (EXFO) and Fluo-3 emitted light was filtered through a band pass 535 +/- 20nm emission filter and detected via a PMT400 photomultiplier sub-system. Simultaneous measurements of sarcomere length were performed as described previously.

RNA-seq: Cardiomyocytes were isolated and concentrated from adult rat hearts as indicated above and split into separate wells as replicates for treatment conditions. After treatment, whole RNA was isolated using RNeasy (Molecular Research Center RN 190) following their standard protocol and snap frozen using liquid nitrogen. Samples were sequenced at Genewiz using Illumina HiSeq 2 x 150 bp after polyA selection. RNA-seq reads were aligned to rat rn6 genome and then gene counts were obtained with STAR (34) using Ensembl Rn6 gene annotation file. Raw counts were transformed to counts per million(CPM) using cpm function with TMM method as implemented in EdgeR (version 3.8.6) (35). Genes with less than 1 CPM in less than 25% of the samples were removed from the analysis. Limma (version 3.4) (36) was used to log2CPM transform the data and test for differential expression. Workflow is similar to limma manual section 9.3. Lmfit function was used to fit a linear model. Contrasts were added with the contrasts.fit function. Finally, differential expression calculation was performed via eBayes function. All were performed with default settings. TopTable function with n=Inf and p.value=1 parameters was used to output the results of each contrast. The default multiple correction method for TopTable function is

Benjamini and Hochberg (“BH”) method (37). Genes with $\log_2FC \geq |1|$ and an adjusted p-value < 0.05 were deemed differentially expressed. Gene Ontology analysis of gene lists was performed using PANTHER(version 14) (38) web-based tool using default settings.

ChIP-seq: LaminB ChIP and subsequent library preparation was performed from control and desmin KD adult rat ventricular myocytes using 2 ug antibody (Lamin B: Abcam, Ab16048) as previously described (39). After preparation of libraries and quantization of ChIP and input DNA, sequencing was performed using an Illumina NextSeq500 machine (vII; 75bp single end sequencing). 75bp Illumina single end reads were trimmed using Trimmomatic (version 0.32) (40) and aligned with bwa (version 0.7.17-r1188) (41) (aln -q 5 -l 32 -k 2) to the Rn6 genome. PCR duplicates were removed with Picard (version 2.9.0) (<http://broadinstitute.github.io/picard>) (VALIDATION_STRINGENCY=LENIENT ASSUME_SORTED=true REMOVE_DUPLICATES=true), multi-mapping reads and reads with a MAPQ score of < 30 were removed using samtools (version 1.7) (42) (-F 1804 -q 30). Three biological replicates of input and paired LB ChIP-seq were sequenced. The number of uniquely mapped read in each replicate pair (ChIP; input) are as follows: Control replicate 1: 14,696,080; 26,176,914, Control replicate 2: 18,204,976; 25,875,923, Control replicate 3: 7,288,192, 11,883,588, desmin KD replicate 1: 130,203; 15,207,304, desmin KD replicate 2: 8,184,660; 21,269,720, desmin KD replicate 3: 128,266, 99,713,838. Spearman correlation coefficients of occupancy across chr1 were calculated between replicates.

Replicate bam files were used as input into Deeptools (version 3.0.2) (43) bamCoverage and converted to bigwig format (--normalizeUsing RPGC --effectiveGenomeSize 2729860805 - bs 10 -e 200). These bigwig files were then input into Deeptools multiBigwigSummary using default settings and region limited to chr1. Resulting data matrix was input into Deeptools plotHeatmap.

After confirming high correlation among input and LB ChIP-seq replicates from control samples, replicate bam files for each treatment were merged. Control LB ChIP and Input replicate libraries were sampled to approximately even depth using samtools. Control LB and Input merged bam files were sampled to ~40 million reads. desmin KD LB and Input bam files were set to ~8 million reads due to low sequencing depth of desmin KD LB. Merged Input normalized coverage tracks for Control and desmin KD treatments were generated using Deeptools bamCompare(--normalizeUsing RPGC --effectiveGenomeSize 2729860805 - bs 10 -e 200) resulting in control lamB and desmin D lamB tracks and are composed of sequencing data from all replicates. To call LADs, merged bam files were converted to bed format using bedtools(version 2.27.1) (44) bamtobed and extended to 200bp using bedtools slop. Bed files were then input to epic (version 0.2.9) (45), and ran with window 600, gap 4, fdr <0.05, rn6 genome and -fs 200 parameters. Resulting peaks within 50kb were merged using bedtools merge, and all peaks <50kb were removed. Control LADs and the Rn6 ENSEMBL gtf file were input to bedtools intersect to identify all features that are contained in LADs, with a minimum of 1bp of any exon/CDS in a LAD.

Electron microscopy: Isolated cardiomyocytes were fixed using 5% glutaraldehyde in 0.2M cacodylate buffer (pH 7.2, EMS 11654) overnight and stored for up to 1 week. Samples were then subjected to triplicate washout of glutaraldehyde, 40-minute staining with 4% osmium tetroxide and washout with DI water. Following two additional washes in sodium acetate buffer (pH 4.2, EMS 11482-42), samples were stained for 2 hours with 8% uranyl acetate. Dehydration was accomplished by 10-minute washes in 70, 95 and 100% ethanol, followed by duplicate 1-hour washes in 100% acetone. Sample was infiltrated with 1:1 EPON acetone mix for 1 hour, then myocytes were selected and arranged in a thin layer on film. Vacuum removal of acetone for 10 minutes, followed by overnight polymerization in an oven resulted in a dense coplanar raft of myocytes which were embedded into an EPON plug and cut into ~70 nm sections using a diamond knife. These sections were collected on copper grids (EMS G200H-Cu) briefly heated to promote adherence and then stained using a modified formulation of Sato lead solution (46). TEM images of nuclei were collected on JEOL 1010 through the University of Pennsylvania Electron Microscopy Resource Lab at 7500x for overall morphology, then at 30000x and 75000x to confirm membrane details.

Nuclear outlines were traced on 7500x images, using higher mag images to confirm the path of the double membrane. Structures where no such membrane was apparent were excluded from the analysis, and regions obscured by the grid or fractures in the sample section were traversed by the shortest straight line. Several desmin knockdown treated nuclei were fully bisected in the plane of the

section. These fragments were traced separately, then combined into a single unit. The convex hull of the nuclear membrane traces was calculated using FIJI and tortuosity calculated as the ratio of the perimeter of the membrane trace to the perimeter of the hull. Distance maps of the convex hull and membrane traces were also calculated in FIJI and used to measure the depth of membranous infolds and segment the interior of the nuclei into depth-coded shells for density measurements. Membranous infolds less than 70nm in depth from the convex hull were excluded from analysis. For the purposes of density measurements, the minimum and maximum values from selected regions within the nucleus were used for normalization to compensate for heterogeneity in staining.

Representative images shown in the manuscript were selected due to their staining quality and to best describe the average phenotype displayed (i.e. not the top/bottom 10 percent of samples).

Whole animal studies: Male and female P4/P5 Sprague Dawley rats were injected either subcutaneously behind the neck or pericardially with either 2.4e10 gc/g of AAV9-shDesmin-BFP (pups were between 8-10 g each) or saline. Rats were allowed to age to adulthood (~5/6 weeks) and blood/tissues were harvested (heart, quad, diaphragm, liver). There were no overt changes in behavior or body weight noted in the experimental rats when compared to their littermates regardless of sex or delivery method. As both pericardial and subcutaneous injection methods gave similar levels of desmin knockdown and changes in nuclear morphology, data was pooled for analysis. Nuclear morphology also

changed similarly in male and female rats upon desmin depletion. Inclusion criteria for these rats required that they be from the same litter, alive/healthy and from the Sprague Dawley strain. Animals with obvious health issues at the time of injection were excluded from this study. Animals were randomized into either treatment or control groups and were assigned numbers that the researcher was blind to until the end of the study.

Statistics: Statistical analysis was performed using OriginPro (Version 9 and 2018). Statistical tests and information on biologic and technical replicates can be found in the figure legend; unless otherwise noted, “N” indicates the number of rat hearts used for independent experiments, while “n” indicates the number of cardiomyocytes or nuclei analyzed. Each adult cardiomyocyte is cultured in isolation from its neighbors (Fig. 1D) and exhibits unique and independent cytoarchitecture and nuclear morphology, as well as variable levels of viral transduction and target depletion upon shRNA delivery. As such each adult cardiomyocyte is treated as an independent biological sample, and experimental observations are always replicated on multiple cell isolations from individual rats. For box plots, the mean line is shown, with whiskers denoting 1 standard deviation (SD) from the mean. For statistical significance, * = $p < 0.05$, ** = $p < 0.01$, *** = $p < 0.001$ vs. control; # = $p < 0.05$, ## = $p < 0.01$, ### = $p < 0.001$ vs. desmin or nesprin-3 depletion, unless otherwise specified in the figure legend. Statistical tests for each comparison are denoted in the figure legends. Unless otherwise specified, normality was tested using a K-squared goodness-of-fit test.

CHAPTER 2: DESMIN AND MICROTUBULES MAINTAIN NUCLEAR STRUCTURE AND GENOME ORGANIZATION

Portions adapted from (78): Heffler, J., Shah, PP., Robison, P., Phyo, S., Veliz, K., Uchida, K., Bogush, A., Rhoades, J., Jain, R. and Prosser, BL. A Balance Between Intermediate Filaments and Microtubules Maintains Nuclear Architecture in the Cardiomyocyte. Circulation Research. 2019;126:e10-e26. doi: 10.1161/CIRCRESAHA.119.315582Ci

Modulation of the cytoskeleton alters nuclear morphology.

The cytoarchitecture and proximity of cytoskeletal elements to the nucleus differs in mature cardiomyocytes from that of non-muscle cells. While non-sarcomeric actin is present in the cardiomyocyte (47), actin stress fibers or TAN lines have not been observed in mature cardiomyocytes. In contrast, both desmin and microtubules exist in close proximity to the cardiomyocyte nucleus (30, 48). Structured illumination microscopy (SIM) images (Figure 1A) demonstrate microtubules running predominantly along the long axis of the cardiomyocyte and forming a cage around the nucleus, which resides in the interior of the myocyte. Desmin intermediate filaments run predominantly along the short axis of the cardiomyocyte at the level of the sarcomeric z-disc and form lateral connections at the nuclear membrane (Figure 1A). To assess if any of these components (actin, desmin, microtubules) are important for regulating baseline nuclear morphology, we used pharmacological and genetic tools to disrupt each of these individually and assessed nuclear dimensions in primary, adult, terminally

differentiated rat ventricular cardiomyocytes. Inhibition of actomyosin tension with ROCK/Rho inhibitors (Y16 and Y27632), which often leads to nuclear rounding in non-muscle cells (49-50), had no effect on baseline nuclear morphology (Figure 1B-C). Depolymerization of actin with latrunculin A (Lat A, 10 μ M for 24hrs) mildly increased nuclear width, with no significant differences detected in length, height, or volume (Figure 1C).

In contrast, disruption of the microtubule network via colchicine (Figure 1C, Colch, 1 μ M for 24hrs) caused an increase in nuclear length, consistent with previous descriptions of microtubules providing compressive force on the nucleus (51). This increase in length was met with a corresponding decrease in height and width and a modest decrease in nuclear volume. In non-muscle cells, microtubule depolymerization can activate RhoA signaling to increase actomyosin-dependent compression on the nucleus (52). To determine if activated RhoA caused the nuclear elongation we observed with microtubule depolymerization, we inhibited RhoA with Y27632 and again treated cells with colchicine. We observed no prevention of the colchicine-dependent changes to nuclear morphology (Figure 1C, lower middle panel), indicating that Rho signaling was unlikely causing the compression we observed, and instead implicating a direct compressive force applied to the nucleus by microtubules.

To assess the role of intermediate filaments, we developed genetic tools to acutely knockdown desmin. We generated shRNAs against desmin (“desmin KD”), introduced them into adenovirus, and transduced adult rat cardiomyocytes *in vitro*. After 48 hours, approximately 50-75 percent of desmin protein was

depleted (Supplemental Figure 1A). Desmin RNA was reduced ~20 fold and was comfortably the most downregulated gene in the transcriptome (as shown later in Figure 9). To our surprise, acute desmin depletion led to a ~50 percent decrease in nuclear volume, predominantly driven by a decrease in nuclear height and width (Figure 1B-C). Taken together, this data suggests desmin maintains nuclear size, perhaps via tension applied along the short axis of the nucleus, while microtubules provide compression along the long axis, and non-sarcomeric actin plays a minimal basal role.

Importantly, these changes in nuclear size were independent of any change in cell size upon desmin or microtubule manipulation. Under our culture conditions, cardiomyocytes are stable morphologically and functionally for at least 72 hours, and only rod-shaped (aspect ratio >3:1) myocytes with preserved membrane morphology (striations) are used for analysis. Cardiomyocyte length, width, or viability were unchanged by the addition of adenovirus encoding a scramble construct or desmin shRNA (Figure 1D), and colchicine treatment similarly had no effect on myocyte size (Supplemental Figure 1B). Thus, desmin depletion causes a specific nuclear involution within a static cell frame.

Acute desmin depletion causes nuclear infolding and chromatin compaction.

We next evaluated this nuclear involution more closely by examining nuclear architecture using super-resolution imaging and electron microscopy. First, we performed immunofluorescence on the intermediate filaments that compose the nuclear lamina: lamin A/C and lamin B1. Desmin depleted cells showed severe

lamina wrinkling and infolding (Figure 2A), which was present in greater than 95 percent of nuclei observed (lower panel, Figure 2B) as assessed by our blinded scoring system (upper panel, Figure 2B). To characterize lamina infolding in live cells, we developed an adenovirus encoding lamin B1-mCherry and co-transduced the virus with either scrambled or desmin KD constructs. At approximately 30 hours post-transduction with shRNA, we performed 10 hr time lapse imaging of infected cardiomyocyte nuclei (Figure 2C, Online Movie 1 and 2). In desmin-depleted cardiomyocytes, discrete sections of the lamina appear to fold inward as the nucleus itself progressively collapses over several hours (white arrows, Figure 2C). To further assess the nature of the folds, we performed electron microscopy (Figure 2D). In desmin-depleted cardiomyocytes, infolds ran deep into the nucleus and were accompanied by the double-membrane nuclear envelope (see high magnification inset on the right-hand side). Quantification of EM images (see Online Movie 3 and 4) revealed a four-fold increase in the infolded area in desmin KD cells (Fig 2E, top). Additionally, while electron-dense heterochromatin was typically restricted to the nuclear periphery and nucleolus in scramble cells (Figure 2D), we observed a considerable extension of the electron-dense chromatin layer – interpreted as heterochromatin - deep into the nuclear interior with desmin depletion (Figure 2D-E). This may reflect chromatin compaction as a result of nuclear involution, or a proliferation of heterochromatin.

Depletion of nesprin-3 phenocopies the nuclear involution seen upon desmin depletion.

We next conducted studies to explore potential mechanisms of desmin's protection of nuclear morphology. Multiple interactions between desmin and the nucleus have been proposed: nesprin-3, encoded by SYNE3, binds to plectin (53-54), which binds to intermediate filaments including desmin (Figure 2F) (53, 55), but LINC-independent interactions between desmin and the nucleus have also been suggested (55). We hypothesized that if desmin interacted with the nucleus via nesprin-3, then depletion of nesprin-3 would phenocopy desmin KD and cause nuclear involution. We generated three shRNA constructs targeted against different regions of nesprin-3 ("nesp-3 KD", Supplemental Figure 2A). After 48hrs of adenoviral transduction all three shRNA variants robustly reduced nesprin-3 protein expression by ~80-90 percent, and we confirmed transcript knockdown via RT-qPCR and western blot (Figure 2F, Supplemental Figure 2B-C). Indeed, all three nesprin-3 KD variants drove a similar nuclear collapse and severe lamina infolding as we observed upon desmin depletion (Figure 2G and Supplemental Figure 3 A-B), consistent with desmin interacting with the nucleus via nesprin-3 to protect against involution.

Nuclear infolding is driven by dynamic microtubules.

We next sought to determine the cause of nuclear involution. Microtubules can provide compressive forces on nuclei (Fig. 1B-C), and previous work has mapped multiple interactions between microtubules and nesprins-1/2 in muscle cells (8, 56). As we also noted that microtubules were often present at sites of nuclear infolding (Figure 3A), we hypothesized that lamina infolding may be

driven by microtubules compressing the nucleus, which is exacerbated in the absence of desmin/nesprin-3. To test this hypothesis, we treated desmin and nesprin-3 KD cardiomyocytes with colchicine to depolymerize microtubules prior to the onset of overt nuclear infolding (see design schematic in Figure 3B and effect of colchicine on microtubules in Figure 3C). Despite confirmation that shRNA-mediated KD was not disrupted by colchicine treatment (Supplemental Figure 2D-E), nuclear infolding and involution was largely prevented when microtubules were depolymerized in desmin or nesprin-3 KD cardiomyocytes (Figure 3D). This result was confirmed for each of the 3 nesprin-3 shRNA variants (Supplemental Figure 3A-B).

Treatment with Latrunculin A did not prevent infold formation (Supplemental Fig 4B), and treatment with colchicine after the folds had formed (Supplemental Fig 4C) did not reverse the infolding phenotype, suggesting that folds are microtubule specific and, once formed, are not readily reversible. Further, neither desmin depletion nor colchicine treatment altered the expression of lamin A/C or lamin B1 (Supplemental Figure 4C), suggesting that a changing composition of the nuclear lamina is unlikely to explain nuclear infolding (or prevention thereof).

We also sought visual confirmation of microtubule-dependent nuclear infolding. To this end, we triple-transduced cells with lamin B1-mCherry, EMTB-3xGFP (to demarcate microtubules), and scramble or desmin KD adenovirus. We observed concurrent formation of lamina infolds with microtubule protrusion into desmin KD nuclei, but no such infolding in scramble nuclei, despite the presence of the perinuclear microtubule cage (Online Movies 5-6).

These visual observations suggested that growing, dynamic microtubules are driving nuclear infolding upon loss of desmin/nesprin-3 tethering to the nucleus. To further test this hypothesis, and to control for off-target consequences of gross microtubule loss upon colchicine treatment, we performed additional experiments with the microtubule-targeting drugs taxol and nocodazole. Nocodazole (at low concentrations) sequesters free tubulin to selectively reduce dynamic microtubule populations, while largely preserving stable, long-lasting microtubules. In contrast, taxol stabilizes and polymerizes microtubules, but also eventually reduces microtubule dynamicity by forcing tubulin into the polymerized pool. The different effects of these three pharmacologic agents on cardiac microtubules can be visualized in Figure 3C. Strikingly, both taxol and nocodazole conferred robust protection from nuclear infolding in desmin-KD cardiomyocytes, despite the remaining presence of a stable cage of microtubules encircling the nucleus, as seen in Figure 3E. This suggests that it is the dynamic growth of microtubules – and not the density of the network per se – that underlies nuclear involution upon desmin depletion.

If nuclear involution requires microtubule interaction with nesprins-1/2, then disrupting this interaction should also prevent nuclear involution. Acute depletion of the genes encoding nesprins-1/2 is challenging due to their large size and high degree of splicing. As an alternative approach, we generated adenovirus over-expressing a dominant-negative KASH peptide (DN-KASH), which disrupts the interaction between nesprins and SUN proteins (6) to disrupt all cytoskeletal-LINC interactions (Supplemental Figure 5A). Consistent with previous reports (6),

we confirmed that the typical perinuclear ring localization of nesprins-1, -2, and -3 was disrupted upon DN-KASH expression (Supplemental Figure 5B-C). If involution requires microtubule interaction with nesprins-1/2 (9), involution should be prevented by DN-KASH (even in the absence of desmin or nesprin-3). Alternatively, if involution does not occur through nesprins-1/2, then DN-KASH should itself cause involution due to the disruption of nesprin-3 and desmin. We found that DN-KASH did not cause involution, but instead nuclei expanded in all axes and increased in volume (Supplemental Figure 5D-E). Moreover, the nuclear lamina did not display infolding, and in fact was even less distorted than control nuclei (Supplemental Figure 5E, IF on left and grading on right). Further, nuclear infolding caused by either desmin or nesprin-3 depletion was largely prevented by co-expression of DN-KASH (Supplemental Figure 5F). Together, these results implicate a model where microtubules interacting with nesprin-1 and/or -2 drive nuclear infolding, which is normally resisted by desmin and nesprin-3. However, given the reliance on the DN-KASH construct, additional experiments will be required to precisely define any interactions between microtubules and the various splice forms of nesprins-1 and -2.

Desmin depletion leads to DNA damage.

Given the gross disruption of nuclear morphology upon desmin depletion, we sought to determine if this was associated with DNA damage. γ H2AX, an indicator of double-stranded DNA breaks, dramatically increased upon desmin depletion. This DNA-damage was significantly prevented by microtubule

depolymerization, as quantified via both immunofluorescence and western blot (Figure 4A-C). The shape change that occurred upon desmin KD was also rescued with colchicine treatment (Figure 4B). We noted that several desmin KD nuclei with preserved size and morphology after colchicine treatment still had elevated levels of γ H2AX, suggesting that the DNA damage observed in this model did not require involution. However, there was a strong positive correlation between nuclear collapse and increased DNA damage, as the γ H2AX signal increased exponentially with a decrease in nuclear size in desmin depleted myocytes (Figure 4D, left). No such correlation was seen in scramble nuclei (Figure 4D, right). Taken together, these data are consistent with a model where desmin-nesprin-3 tethering of the nucleus protects it from microtubule-dependent infolding, collapse, and DNA damage.

DN-KASH causes DNA damage.

As previously noted, we observed that even normally shaped and unwrinkled nuclei showed an elevation in γ H2AX with colchicine and desmin KD co-treatment. We hypothesized this was due to baseline connections between the cytoskeletal and LINC network being an important regulatory network for the DNA-damage response in adult cardiomyocytes. To begin testing this, we hypothesized that DN-KASH ought to phenocopy the elevation in γ H2AX signal we had seen with desmin KD and microtubule disruption. Indeed, as shown by IF and quantified (Figure 5A-B), treatment with DN KASH alone does elevate γ H2AX. We next hypothesized that if this increase in γ H2AX was caused by

sarcomeric tension in the cell, treatment with blebbistatin would reduce the amount of DNA damage we were observing. Treatment with blebbistatin caused a trend toward a lower overall signal intensity but this was not significant. Additionally, we noted that the number of γ H2AX particles detected was unchanged, implying the difference in signal intensity was more intense γ H2AX puncta versus more puncta (Figure 5A-B).

Desmin depletion disrupts nuclear homeostasis *in vivo* and *in situ*.

As the forces imposed on cardiomyocyte nuclei will differ in beating tissue compared to isolated cardiomyocytes, we next used two approaches to investigate desmin's nuclear protection *in situ*. Per the original characterizations by Milner et al. and Li et al., desmin knock-out mice exhibit severe defects in myocardial architecture and cardiomyopathy (26, 57), making it difficult to interpret any nuclear phenotype (58) as primary to the loss of desmin or secondary to disease pathology. We thus sought to deplete desmin in a minority of cardiomyocytes *in vivo*, which was accomplished via the generation and transduction of a low-dose of AAV9 encoding shRNA against desmin. We injected both male and female P4/5 rats with AAV9-shDesmin-BFP (KD) or saline (sham) at a viral dosage that achieved 30.1 +/- 4.8% transduction efficiency of cardiomyocytes. After 5 weeks, we extracted the hearts from these rats and performed tissue sectioning and immunofluorescence imaging. As expected, we observed desmin expression only in cardiac myocytes, and KD hearts demonstrated mild tissue disorganization. Fortunately, most cardiomyocytes

could be identified as either clearly positive or clearly negative for desmin immuno-reactivity (Figure 6A-B). We thus compared nuclei in desmin-negative myocytes to two controls: myocyte nuclei from sham-injected hearts, and from internal, tissue-matched desmin-positive controls. Using cTNT labeling to identify cardiomyocyte nuclei, nuclei were traced to obtain size parameters, and scored blindly by two independent observers to quantify morphology defects. Upon desmin depletion, nuclei were shorter, rounder, and had significantly more morphological defects (Figure 6B-C). In KD hearts, cardiomyocytes still containing desmin had nuclei that were morphologically more like their sham counterparts than their desmin-depleted neighbors (Figure 6B-C), supporting a primary role of desmin in maintaining nuclear architecture *in vivo*.

Due to practical limitations of organ level experiments, we also sought to establish a parallel, more flexible platform to interrogate the interplay between microtubules and intermediate filaments in loaded, beating cardiac syncytia. To this end we co-cultured neonatal rat ventricular myocytes (NRVMs) and cardiac fibroblasts on aligned, nano-patterned substrates that promote tissue maturation and syncytial formation (Figure 7A, upper panel). Within 48hrs of plating on patterned substrates, the tissue is robustly aligned along the pattern axis and exhibits improved maturation compared to un-patterned cells. This is demonstrated by improved myofibril alignment, uniaxial beating, and, importantly, cytoarchitecture reminiscent of mature cardiac tissue (Figure 7A, lower panels). Of note, the organization of desmin into a striated, transverse structure is strongly promoted by tissue patterning. Three days post-plating tissues were

infected with adenovirus encoding either control shRNA or shRNA targeted toward desmin and nuclear phenotypes were assessed. Upon desmin KD, α -actinin organization was still evident but slightly misaligned, and transverse desmin filaments were no longer observed (Figure 7B). Despite the modest change in sarcomeric architecture, nuclear morphology was significantly compromised (Figure 7C). As in unloaded adult myocytes, desmin KD drove involution and infolding of nuclei in beating NRVM syncytia, as well as a robust increase in DNA damage. Colchicine treatment to depolymerize microtubules reduced DNA damage and fully protected from the morphological abnormalities induced by desmin depletion (Figure 7C-D). Together with the above, this data indicates that desmin protects against microtubule-dependent disruption of nuclear homeostasis *in situ*.

Acute reduction in desmin via dTAG degron causes nuclear involution in mice.

One phenotype of note when performing the AAV9 experiments discussed above was that normal, control virus elicited inflammatory and hypertrophic response, required a large amount of virus which was practically expensive, while also not providing us with 100 percent protein reduction. Because of these limitations, we sought a method of acutely reducing desmin that 1) would not allow for compensatory changes to other intermediate filaments and 2) would completely reduce the protein in the heart. To these ends, we began a collaboration with the Grey lab that had been perfecting a protein degradation system to acutely eliminate specific proteins of interest from a cell.

The dTAG system works by chimerically fusing a protein of interest to a FKBP^{F36V} and knocking this chimeric allele into the endogenous locus of a mouse using CRISPR. In the absence of the heterobifunctional degrader (dTAGv1 or BNN), this chimeric allele functions normally. Once added, BNN causes recruitment of the E3 ubiquitin ligase (VHL, CRBN) to the BET bromodomain of the FKBP, causing subsequent ubiquitination and rapid degradation of the protein (59-60).

We received confirmation that the construct worked (genotyping gel not shown) and bred the mice to have homozygous knock-ins of the mutant allele. After 22 hours at 500 nM BNN, we were able to observe nearly 99 percent reduction in desmin-FKBP^{F36V} protein levels (Figure 8A).

Next, we sought to do immunofluorescence to determine if 1) loss of desmin could be observed via IF and 2) if acute reduction of desmin-FKBP^{F36V} would result in misshapen nuclei. Indeed, we observed a trend toward rounded, more wrinkled nuclei after desmin-FKBP degradation; however, the blinded grading failed to reach significance due to low sample size (Figure 8B-C).

While these data are incomplete, we are hoping to repeat these experiments and move toward a whole-animal study of the effect of acute desmin reduction in the heart.

CHAPTER 3: FUNCTIONAL CONSEQUENCES OF ACUTE DESMIN

DEPLETION

Portions adapted from (78): Heffler, J., Shah, PP., Robison, P., Phyo, S., Veliz, K., Uchida, K., Bogush, A., Rhoades, J., Jain, R. and Prosser, BL. A Balance Between Intermediate Filaments and Microtubules Maintains Nuclear Architecture in the Cardiomyocyte. Circulation Research. 2019;126:e10-e26. doi: 10.1161/CIRCRESAHA.119.315582Ci

Desmin depletion drives large-scale changes to gene expression and compromises lamina-associated chromatin.

As DNA damage is a well-established response to a loss of genome-organization (61-63), we next assessed the genomic and transcriptomic consequences of desmin depletion. RNA sequencing revealed many differentially expressed genes between scramble and desmin KD cardiomyocytes (Figure 9A), with approximately 20% of the genome differentially regulated following desmin depletion (at a cutoff of > 2-fold change, adj. p-value <0.05). Fortuitously, desmin KD did not significantly affect the expression of any of the Nesprin or SUN isoforms detected in cardiomyocytes, simplifying the interpretation of experiments manipulating the LINC complex. Bioinformatic analysis of these differentially expressed genes indicated that the most significantly altered gene ontology (GO) groups encoded transcripts involved in ion handling, contractility and mitochondrial function and metabolism, functional groups previously noted to be altered with misregulation of desmin. Moreover, acute desmin depletion

produced a genetic signature highly associated with cardiac dysfunction, hypertrophy, and dilated cardiomyopathy (Figure 9B), consistent with known phenotypes caused by desmin mutations.

Given the disruption of lamina architecture (Figure 2), we hypothesized that the desmin-dependent loss of genome organization may arise from disruption of lamina-associated chromatin domains. We thus assessed LADs by performing lamin B chromatin immunoprecipitation followed by sequencing (LB ChIP-seq). We first confirmed our ability to specifically ChIP lamin B from rat cardiomyocytes (Supplemental Figure 6A). We then performed LB ChIP-seq from three independent pools of scramble-treated cardiomyocytes. After confirming high correlation between the input and ChIP replicates (Supplemental Figure 6B), we merged replicate data, input normalized LB ChIP-seq data, and defined LADs using an unbiased algorithm (64) (Figure 9C, Supplemental Figure 6C). Like LADs in cardiomyocytes and other cell types from different model species (39, 45, 65-66), rat cardiomyocyte LADs encompass approximately 40 percent of the genome and house 7561 genes and features (Supplemental Figure 6C).

We further confirmed lamin B expression and our ability to ChIP lamin B in desmin-depleted cells (Supplemental Figure 6B); however, LB-ChIP in desmin-depleted cells resulted in only a fraction of enriched chromatin compared to scramble control, despite normal levels of LaminB1. Thus, three biological LB ChIP-seq replicates resulted in fewer than 8.6M uniquely mapping reads, compared to over 40M for the control samples using the same amount of starting material for ChIP. This suggests that desmin-depletion compromises normal

chromatin enrichment to lamin B. Given the low number of reads, it was not feasible to define LADs in KD cardiomyocytes; however, we note that the input-normalized LB ChIP-seq reads from desmin-KD cells are localized in LAD regions (as defined in scramble cardiomyocytes; Figure 9C – compare bottom vs. top tracks), further supporting the hypothesis that LAD structure and LaminB1-chromatin interactions are compromised upon desmin depletion.

Finally, we determined the impact of the potential “LAD loss” on gene transcription. Genes in LADs are preferentially transcriptionally repressed compared to those not in LADs (45); consistently, we observed that genes found in control cardiomyocyte LADs tended to be up-regulated when “lost” from LADs upon desmin KD, while genes not found in LADs were significantly more likely to be down-regulated upon desmin depletion (Figure 9D-E). Together, this data indicates that acute loss of desmin rapidly compromises genome organization in the cardiomyocyte, with broad consequences on the cardiac transcriptome.

Acute Desmin Depletion Disrupts Excitation-Contraction Coupling

Given the marked genomic and transcriptomic changes, particularly in genes involved in calcium handling and contractility, we next assessed excitation-contraction (EC) coupling and cell shortening in desmin KD myocytes. As desmin may regulate EC coupling through a variety of mechanisms, we also interrogated these metrics in nesprin-3 depleted cells to better isolate an effect of disrupting the desmin-nesprin3 axis. Cardiomyocytes depleted of either desmin or nesprin-3 displayed altered calcium transients (Figure 10A) and contractility (Figure 10C)

upon electrical stimulation. Consistent with the differential expression of multiple transcripts integral to the maintenance of a normal calcium transient (e.g., *serca2a*, *ryr2*, *pln*), desmin KD myocytes demonstrated briefer cytosolic calcium transients, with a faster decay of the calcium transient, and this was accompanied by briefer contractions and less cell shortening (Figure 10A-D, red). Nesprin-3 depleted myocytes exhibited similar changes to calcium handling and contractility (Figure 10A-D, blue), suggesting that at least part of desmin's regulation of EC coupling likely arises from its role at the nucleus. Together, these data demonstrate significant and rapid alterations in cardiomyocyte function with acute disruption of desmin or nesprin-3, suggesting that cytoskeletal coupling to the LINC complex helps maintain normal EC coupling.

Acute Desmin Depletion Alters Cellular Stiffness and Microtubule Buckling

Previous work from the Prosser lab has shown that post-translational modification of α -tubulin via the cleavage of the C-terminal tyrosine ("detyrosination" or "dTyr") is an important factor for regulating the stiffness of the cardiomyocyte (21, 30). This process has been hypothesized to occur via a linkage between these dTyr microtubules and the intermediate filament desmin at the z-disc. This interaction creates an increase in viscosity during contraction in the cardiomyocyte by inducing microtubule buckling (30). While the previous paper sought to explore the microtubule-modification side of this hypothesis, we continued to look at the z-disc/desmin side to see if the knockdown of desmin

could also phenocopy the changes to buckling and viscosity we had previously observed with changes to dTyr microtubules.

Upon desmin reduction, cardiomyocytes show a significant decrease in viscosity, as indicated by the change in primarily the fast indentation regime as measured by atomic force microscopy (AFM) (Figure 11A-B). This change in viscosity is also associated with changes to the buckling properties of the microtubules. While the microtubules in desmin KD cardiomyocytes do still buckle, they tend to buckle a wavelength much higher than that of contracted sarcomere (1.9 μm vs 1.5-1.7 μm) (Figure 12A-B). Moreover, data from another member of the lab has shown that microtubules in desmin KD cardiomyocytes tend to pause less frequently at the z-disc and have a greater incidence of catastrophe on the z-disc than they would otherwise (67) implying a loss of a stabilizing connection at that site.

Lastly, we sought to characterize the relative amounts of dTyr versus Tyr microtubules after desmin KD. We observed that for both dTyr and Tyr microtubules, the fractional area covered was decreased, implying a loss in the overall microtubule network (Figure 13A-B), which is consistent with the hypothesis that desmin serves as a stabilizing structure to the microtubule network.

How desmin specifically causes changes to the microtubule network is unclear; however, we can speculate from these data that there is feedback between the desmin intermediate filament and microtubule networks that affect cell stiffness, microtubule stability and overall homeostasis.

CHAPTER 4: DISCUSSION AND FUTURE DIRECTIONS

Portions adapted from (78): Heffler, J., Shah, PP., Robison, P., Phyto, S., Veliz, K., Uchida, K., Bogush, A., Rhoades, J., Jain, R. and Prosser, BL. A Balance Between Intermediate Filaments and Microtubules Maintains Nuclear Architecture in the Cardiomyocyte. Circulation Research. 2019;126:e10-e26. doi: 10.1161/CIRCRESAHA.119.315582Ci

From this work we conclude that the intermediate filament desmin preserves nuclear homeostasis in cardiac muscle cells via its interactions with the LINC complex. Desmin and microtubules form a filamentous meshwork around the cardiomyocyte nucleus, largely consisting of axial microtubules and transverse intermediate filaments. Here we find that they maintain nuclear shape and size and help preserve the architecture of the nuclear lamina and its associated chromatin-interacting domains. Acute depletion of desmin causes rapid nuclear involution, infolding of the nuclear envelope and lamina, and DNA damage that are driven by dynamic microtubules. Desmin depletion drives the loss of chromatin enrichment at the nuclear lamina and large transcriptomic changes that are concomitant with impaired cardiomyocyte function. Intriguingly, loss of nesprin connections to the cytoskeleton appear to be sufficient to increase DNA damage levels as measured by γ H2AX with a possible tie to sarcomeric tension. Many of these findings can be seen in not only isolated, individual cardiomyocytes but also pseudo tissue platforms, AAV9-mediated *in vivo* knockdown and now also in desmin-FKBP^{F36V}-forced degradation. Lastly, we

have shown that desmin has an important role in the regulation of the microtubule network and post-translational modification persistence. This translates to an overall less stiff cardiomyocyte and a reduction in overall microtubule coverage. Taken together, we can conclude that desmin has a previously overlooked role in nucleus structure and homeostasis and overall health of the cardiomyocyte.

Multiple, non-exclusive mechanisms may underlie the desmin and microtubule-mediated maintenance of nuclear integrity. First, our data support a model where desmin and microtubules maintain a force-balance on the cardiomyocyte nucleus. Desmin, via attachments to the myofilaments and the nucleus (via nesprin-3), may provide resting tension on the nucleus, resisting compressive loads. Microtubules, on the other hand, compress and contain the nucleus in a cage-like structure, and connect to the outer nuclear membrane via nesprin-1 and/or -2. Upon acute loss of desmin, this force-balance is disrupted, allowing dynamic microtubules to drive infolding of the nuclear envelope. Alternatively, desmin may function as a scaffold to protect the cardiomyocyte nucleus from aberrant microtubule compression. Desmin is required for proper microtubule network organization (30), and under normal conditions desmin may sequester microtubules or guide microtubule growth peripheral to the nucleus, mitigating microtubule compression. A third hypothesis involves the activation of signaling cascades that may structurally weaken the nucleus upon release of desmin. Cytoskeletal tension on the nucleus can stiffen the nuclear lamina both via increasing levels of lamin A/C (68) and via emerin-dependent signaling cascades

(69). Release of desmin or desmin-LINC tension may soften the lamina (70), thus allowing microtubule-dependent forces to more readily involute the nucleus. In the future, direct measurements of the magnitude and directionality of forces imposed on the cardiomyocyte nucleus using discrete force sensors may help discriminate between these models, although they likely are not independent. More work is needed to establish the precise molecular mechanism by which microtubules interact with the outer nuclear membrane and the LINC complex, and whether this interaction is direct or requires specific microtubule associated proteins to drive nuclear infolding.

The situation is further complicated in the mechanical environment of cardiomyocytes *in situ*, which experience a complex mix of compression, strain, torsion, and shear. In both *in situ* and *in vitro* experiments, we observed decreased nuclear length and increased nuclear morphology defects upon desmin depletion. Yet *in vivo* we observed rounding of desmin-depleted nuclei, a phenotype not consistently observed in isolated cardiomyocytes. This could arise from several contextual differences, such as continuous stretch and contraction *in vivo* leading to the rounding of nuclei lacking attachment to the desmin network or the increased time lacking desmin in these hearts.

The differential effects of acute and chronic desmin depletion are also worth consideration. It is unclear if disruption of desmin (or nesprins) is compensated for over time or during development. While germline desmin knockout (KO) mice have been reported to have altered nuclear morphology in skeletal (71) and cardiac muscle (20), underlying mechanisms were not determined, and whether

this was a direct or indirect consequence of the loss of desmin remained unclear. Our data provide a novel, direct mechanism for desmin's nuclear protection. Desmin KO mice display muscle weakness, exercise intolerance (Shah *Biophys J* 2004) and prominent alterations to their transcriptome, particularly in relation to metabolic and mitochondrial gene (19-20, 72), and desmin depleted or mutant zebrafish exhibit defective EC coupling and contractility in skeletal and cardiac muscle (73-74). Intriguingly, we see differential regulation of a variety of metabolic, calcium handling and contractility-associated genes within 48hrs of desmin depletion in adult mammalian cardiomyocytes, and disruption of nesprin-3 produces similar contractile defects. While whole-animal phenotypes are likely multi-factorial due to desmin's promiscuous interactions, disrupting its association with the nucleus should be considered as a potential driver of diverse phenotypic consequences seen upon desmin loss or gain of function.

While several mutations in nesprins-1 and -2 are associated with cardiomyopathy, we are unaware of myopathy-related mutations in nesprin-3. Nesprin-3 KO mice are viable (57), but cardiac phenotypes have not been explored and warrant further study, particularly upon application of mechanical stress. It is also worth noting that nesprin isoforms may compensate for one another during development, as supported by mouse models of nesprin ablation (16).

Considerable remodeling of both the desmin and microtubule networks occur in human heart failure (21, 75). Desmin protein levels are increased 3-5-fold, and desmin is phosphorylated, cleaved and aggregated (27-28). Microtubules also

proliferate and are highly stabilized and detyrosinated, particularly those enriched around the cardiomyocyte nucleus. Future work should interrogate how this cytoskeletal proliferation and post-translational modification affects the relationship between desmin, microtubules and nucleus, and whether this may contribute to altered genome organization and pathology in heart failure. Of note, disruption of lamin A/C, which also causes cardiomyopathy, leads to disorganization of desmin filaments at the nucleus (76). Together with our work, this indicates bi-directional interactions between the desmin and microtubule networks as well as their combinatorial interaction with the overall nucleoskeletal network and how these complex interactions are required to preserve nuclear integrity in the heart.

Cytoskeletal attachments to the nucleus have received considerable attention in recent years as potential sites of mechanotransduction. While much of the work has focused on the coupling of actomyosin stress fibers to the nucleus, little is known regarding the roles of microtubules and intermediate filaments and their interactions with the nucleoskeleton. Microtubule-LINC interactions are required for nuclear positioning in skeletal muscle (8-9), where desmin also plays a role (77), yet the regulation of nuclear mechanotransduction is unexplored. Given their intriguing ability to modulate lamina-associated chromatin, future studies should explore whether microtubules and intermediate filaments are involved in cardiomyocyte mechanosensing and response or merely provide structural reinforcement. Our data suggest that the basal connections between the nesprin and SUN proteins are required to keep the DNA-damage response low,

presumably via maintenance of chromatin organization. Further work will need to determine exactly how this occurs and what proteins are required to mediate this signaling.

In sum, our data indicate that desmin and microtubules form a dense, interconnected network that surrounds the cardiomyocyte nucleus, and, when balanced, maintains nuclear homeostasis. Disruption of endogenous desmin increases the susceptibility of cardiomyocyte nuclei to microtubule-dependent collapse, a loss of genome architecture and DNA damage, and this disruption of nuclear homeostasis is associated with impaired cardiomyocyte function. This work provides mechanistic insight into the role of desmin intermediate filaments and suggests that improper regulation of nuclear integrity may contribute to pathology in desmin-related diseases.

BIBLIOGRAPHY

1. Fan, D., Takawale, A., Lee, J., and Kassiri, Z. Cardiac fibroblasts, fibrosis and extracellular matrix remodeling in heart disease. *Fibrogenesis Tissue Repair*. 2012;5:15. doi: 10.1186/1755-1536-5-15
2. Krueger, W., Bender, N., Haeusler, M., and Henneberg, M. The role of mechanotransduction in heart failure pathobiology—a concise review. *Heart Failure Reviews*. 2020; Jan 22. doi: 10.1007/s10741-020-09915-1
3. Davis, J, Davis, LC, Correll, RN, Makarewich, CA, Schwanekamp, JA, Moussavi-Harami, F, Wang, D, York, AJ, Wu, H, Houser, SR, et al. A tension- based model distinguishes hypertrophic versus dilated cardiomyopathy. *Cell*. 2016;165:1147–1159. doi: 10.1016/j.cell.2016.04.002
4. Szczesny, SE, Mauck, RL. The nuclear option: evidence implicating the cell nucleus in mechanotransduction. *J Biomech Eng*. 2017;139:021006. doi: 10.1115/1.4035350
5. Wong, X., Loo, T., and Steward, C. LINC complex regulation of genome organization and function. *Current Opinion in Genetics & Development*. 2021; 67:130-141. doi:10.1016/j.gde.2020.12.007
6. Lombardi, ML, Jaalouk, DE, Shanahan, CM, Burke, B, Roux, KJ, Lammerding, J. The interaction between nesprins and sun proteins at the nuclear envelope is critical for force transmission between the

- nucleus and cytoskeleton. *J Biol Chem*. 2011;286:26743–26753. doi: 10.1074/jbc.M111.233700
7. Mellad, J., Warren, D., and Shanahan, C. Nesprins LINC the nucleus and cytoskeleton. *Current Opinion in Cell Biology*. 2011;23:47-54. doi: 10.1016/j.ceb.2010.11.006
 8. Wilson, MH, Holzbaur, EL. Nesprins anchor kinesin-1 motors to the nucleus to drive nuclear distribution in muscle cells. *Development*. 2015;142:218–228. doi: 10.1242/dev.114769
 9. Stroud, MJ, Feng, W, Zhang, J, Veevers, J, Fang, X, Gerace, L, Chen, J. Nesprin 1 α 2 is essential for mouse postnatal viability and nuclear positioning in skeletal muscle. *J Cell Biol*. 2017;216:1915–1924. doi: 10.1083/jcb.201612128
 10. Konieczny, P, Fuchs, P, Reipert, S, Kunz, WS, Zeöld, A, Fischer, I, Paulin, D, Schröder, R, Wiche, G. Myofiber integrity depends on desmin network targeting to Z-disks and costameres via distinct plectin isoforms. *J Cell Biol*. 2008;181:667–681. doi: 10.1083/jcb.200711058
 11. Reipert, S, Steinböck, F, Fischer, I, Bittner, RE, Zeöld, A, Wiche, G. Association of mitochondria with plectin and desmin intermediate filaments in striated muscle. *Exp Cell Res*. 1999;252:479–491. doi: 10.1006/excr.1999.4626
 12. Janota, C., Calero-Cuenca, F. J., and Gomes, E.R. The role of the cell nucleus in mechanotransduction. *Current Opinion in Cell Biology*. 2020;63:204-211. doi:10.1016/j.ceb.2020.03.001

13. Tsikitis, M, Galata, Z, Mavroidis, M, Psarras, S, Capetanaki, Y. Intermediate filaments in cardiomyopathy. *Biophys Rev.* 2018;10:1007–1031. doi: 10.1007/s12551-018-0443-2
14. McNally, EM, Golbus, JR, Puckelwartz, MJ. Genetic mutations and mechanisms in dilated cardiomyopathy. *J Clin Invest.* 2013;123:19–26. doi: 10.1172/JCI62862
15. Stroud, MJ. Linker of nucleoskeleton and cytoskeleton complex proteins in cardiomyopathy. *Biophys Rev.* 2018;10:1033–1051. doi: 10.1007/s12551-018-0431-6
16. Banerjee, I, Zhang, J, Moore-Morris, T, Pfeiffer, E, Buchholz, KS, Liu, A, Ouyang, K, Stroud, MJ, Gerace, L, Evans, SM, et al. Targeted ablation of nesprin 1 and nesprin 2 from murine myocardium results in cardiomyopathy, altered nuclear morphology and inhibition of the biomechanical gene response. *PLoS Genet.* 2014;10:e1004114. doi: 10.1371/journal.pgen.1004114
17. Frank, D. and Frey, N. Cardiac Z-disc Signaling Network. *Journal of Biological Chemistry.* 2011;286: 9897-9904. doi: 10.1074/jbc.R110.174268
18. Diokmetzidou, A, Soumaka, E, Kloukina, I, Tsikitis, M, Makridakis, M, Varela, A, Davos, CH, Georgopoulos, S, Anesti, V, Vlahou, A, et al. Desmin and α B-crystallin interplay in the maintenance of mitochondrial homeostasis and cardiomyocyte survival. *J Cell Sci.* 2016;129:3705–3720. doi: 10.1242/jcs.192203

19. Fountoulakis, M, Soumaka, E, Rapti, K, Mavroidis, M, Tsangaris, G, Maris, A, Weisleder, N, Capetanaki, Y. Alterations in the heart mitochondrial proteome in a desmin null heart failure model. *J Mol Cell Cardiol.* 2005;38:461–474. doi: 10.1016/j.yjmcc.2004.12.008
20. Capetanaki, Y, Milner, DJ, Weitzer, G. Desmin in muscle formation and maintenance: knockouts and consequences. *Cell Struct Funct.* 1997;22:103–116. doi: 10.1247/csf.22.103
21. Chen, CY, Caporizzo, MA, Bedi, K, Vite, A, Bogush, AI, Robison, P, Heffler, JG, Salomon, AK, Kelly, NA, Babu, A, et al. Suppression of deetyrosinated microtubules improves cardiomyocyte function in human heart failure. *Nat Med.* 2018;260:682–1233
22. Capetanaki, Y, Bloch, RJ, Kouloumenta, A, Mavroidis, M, Psarras, S. Muscle intermediate filaments and their links to membranes and membranous organelles. *Exp Cell Res.* 2007;313:2063–2076. doi: 10.1016/j.yexcr.2007.03.033
23. Boriek, AM, Capetanaki, Y, Hwang, W, Officer, T, Badshah, M, Rodarte, J, Tidball, JG. Desmin integrates the three-dimensional mechanical properties of muscles. *Am J Physiol Cell Physiol.* 2001;280:C46–C52. doi: 10.1152/ajpcell.2001.280.1.C46
24. Palmisano, MG, Bremner, SN, Hornberger, TA, Meyer, GA, Domenighetti, AA, Shah, SB, Kiss, B, Kellermayer, M, Ryan, AF, Lieber, RL. Skeletal muscle intermediate filaments form a stress-

- transmitting and stress-signaling network. *J Cell Sci.* 2015;128:219–224. doi: 10.1242/jcs.142463
25. van Spaendonck-Zwarts, KY, van Hessem, L, Jongbloed, JD, de Walle, HE, Capetanaki, Y, van der Kooi, AJ, van Langen, IM, van den Berg, MP, van Tintelen, JP. Desmin-related myopathy. *Clin Genet.* 2011;80:354–366. doi: 10.1111/j.1399-0004.2010.01512.x
 26. Milner, DJ, Weitzer, G, Tran, D, Bradley, A, Capetanaki, Y. Disruption of muscle architecture and myocardial degeneration in mice lacking desmin. *J Cell Biol.* 1996;134:1255–1270. doi: 10.1083/jcb.134.5.1255
 27. Agnetti, G, Halperin, VL, Kirk, JA, Chakir, K, Guo, Y, Lund, L, Nicolini, F, Gherli, T, Guarnieri, C, Caldarera, CM, et al. Desmin modifications associate with amyloid-like oligomers deposition in heart failure. *Cardiovasc Res.* 2014;102:24–34. doi: 10.1093/cvr/cvu003
 28. Rainer, PP, Dong, P, Sorge, M, Fert-Bober, J, Holewinski, RJ, Wang, Y, Foss, CA, An, SS, Baracca, A, Solaini, G, et al. Desmin phosphorylation triggers preamyloid oligomers formation and myocyte dysfunction in acquired heart failure. *Circ Res.* 2018;122:e75–e83. doi: 10.1161/CIRCRESAHA.117.312082
 29. McLendon, PM, Robbins, J. Desmin-related cardiomyopathy: an unfolding story. *Am J Physiol Heart Circ Physiol.* 2011;301:H1220–H1228. doi: 10.1152/ajpheart.00601.2011
 30. Robison, P, Caporizzo, MA, Ahmadzadeh, H, Bogush, AI, Chen, CY, Margulies, KB, Shenoy, VB, Prosser, BL. Detyrosinated microtubules

buckle and bear load in contracting cardiomyocytes. *Science*. 2016;352:aaf0659. doi: 10.1126/science.aaf0659

31. Scarborough, E.A., Uchida, K., Vogel, M., Erlitzki, N., Iyer, M., Phyo, S. A., Bogush, A., Kehat, I., and Prosser, B. L. Microtubules orchestrate local translation to enable cardiac growth. *Nature Communications*. 2021;12: 1547. doi: 10.1038/s41467-021-21685-4
32. Prosser, B. L., Ward, C. W., and Ledere, W. J. X-ROS Signaling: Rapid Mechano-Chemo Transduction in Heart. *Science*. 2011;333:1440-1445. doi: 10.1126/science.1202768
33. Prosser BL, Khairallah RJ, Ziman AP, Ward CW, Lederer WJ. X-ROS signaling in the heart and skeletal muscle: stretch-dependent local ROS regulates $[Ca^{2+}]_i$. *J Mol Cell Cardiol*. 2013;58:172-181. doi:10.1016/j.yjmcc.2012.11.011
34. Dobin, A., Davis, CA., Schlesinger, F., Drenkow, J., Zaleski, C., Jha, S., Batut, P., Chaisson, M. and Gingeras, TR. STAR: ultrafast universal RNA-seq aligner. *Bioinformatics*. 2013;29:15-21. doi: 10.1093/bioinformatics/bts635
35. Liao, Y., Smyth, GK. And Shi, W. The Subread aligner: fast, accurate and scalable read mapping by seed-and-vote. *Nucleic Acids Research*. 2013;41:e108. doi:10.1093/nar/gkt214.
36. Robinson, MD., McCarthy, DJ. and Smyth, GK. edgeR: a Bioconductor package for differential expression analysis of digital gene expression

- data. *Bioinformatics*. 2010;26:139-140. doi:
10.1093/bioinformatics/btp616
37. Ritchie, ME., Phipson, B., Wu, D., Hu, Y., Law, CW., Shi, W. and Smyth, GK. limma powers differential expression analyses for RNA-sequencing and microarray studies. *Nucleic Acids Research*. 2015;43:e47. doi: 10.1093/nar/gkv007
38. Mi, H., Huang, X., Muruganujan, A., Tang, H., Mills, C., Kang, D. and Thomas PD. PANTHER version 11: expanded annotation data from Gene Ontology and Reactome pathways, and data analysis tool enhancements. *Nucleic Acids Research*. 2017;45:D183-D189. doi: 10.1093/nar/gkw1138
39. Poleshko, A, Shah, PP, Gupta, M, Babu, A, Morley, MP, Manderfield, LJ, Ifkovits, JL, Calderon, D, Aghajanian, H, Sierra-Pagán, JE, et al. Genome-nuclear lamina interactions regulate cardiac stem cell lineage restriction. *Cell*. 2017;171:573–587.e14. doi: 10.1016/j.cell.2017.09.018
40. Bolder, AM., Lohse, M. and Usadel, B. Trimmomatic: a flexible trimmer for Illumina sequence data. *Bioinformatics*. 2014;30:2114-2120. doi: 10.1093/bioinformatics/btu170
41. Li, H. and Durbin, R. Fast and accurate short read alignment with Burrows–Wheeler transform. *Bioinformatics*. 2009;25:1754-1760. doi: 10.1093/bioinformatics/btp324

42. Li, H., Handsaker, B., Wysoker, A., Fennell, T., Ruan, J., Homer, N., Marth, G., Abecasis, G. and Durbin, R. The Sequence Alignment/Map format and SAMtools. *Bioinformatics*. 2009;25:2078-2079. doi: 10.1093/bioinformatics/btp352
43. Ramírez, F., Ryan, DP., Grüning, B., Bhardwaj, V., Kilpert, F., Richter, AS., Heyne, S., Dündar, F. and Manke, T. deepTools2: a next generation web server for deep-sequencing data analysis. *Nucleic Acids Research*. 2016;44:W160–W165. doi: 10.1093/nar/gkw257
44. Quinlan, AR. And Hall, IM. BEDTools: a flexible suite of utilities for comparing genomic features. *Bioinformatics*. 2010;26:841-842. doi: 10.1093/bioinformatics/btq033
45. Zang, C., Schones, DE., Zeng, C., Cui, K., Zhao, K. and Peng, W. A clustering approach for identification of enriched domains from histone modification ChIP-Seq data. *Bioinformatics*. 2009;25:1952-1958. doi: 10.1093/bioinformatics/btp340
46. Hanaichi, T., Sato, T., Iwamoto, T., Malavasi-Yamashiro, J., Hoshino, M. and Mizuno, N. A Stable Lead by Modification of Sato's Method. *Journal of Electron Microscopy*. 1986;35:304-306. doi: 10.1093/oxfordjournals.jmicro.a050582
47. Kee, AJ, Gunning, PW, Hardeman, EC. Diverse roles of the actin cytoskeleton in striated muscle. *J Muscle Res Cell Motil*. 2009;30:187–197. doi: 10.1007/s10974-009-9193-x

48. Bloom, S, Lockard, VG, Bloom, M. Intermediate filament-mediated stretch-induced changes in chromatin: a hypothesis for growth initiation in cardiac myocytes. *J Mol Cell Cardiol.* 1996;28:2123–2127. doi: 10.1006/jmcc.1996.0204
49. Khatau, SB, Hale, CM, Stewart-Hutchinson, PJ, Patel, MS, Stewart, CL, Searson, PC, Hodzic, D, Wirtz, D. A perinuclear actin cap regulates nuclear shape. *Proc Natl Acad Sci U S A.* 2009;106:19017–19022. doi: 10.1073/pnas.0908686106
50. Versaevel, M, Grevesse, T, Gabriele, S. Spatial coordination between cell and nuclear shape within micropatterned endothelial cells. *Nat Commun.* 2012;3:671. doi: 10.1038/ncomms1668
51. Kim, DH, Li, B, Si, F, Phillip, JM, Wirtz, D, Sun, SX. Volume regulation and shape bifurcation in the cell nucleus. *J Cell Sci.* 2015;128:3375–3385. doi: 10.1242/jcs.166330
52. Park, YH, Wood, G, Kastner, DL, Chae, JJ. Pyrin inflammasome activation and RhoA signaling in the autoinflammatory diseases FMF and HIDS. *Nat Immunol.* 2016;17:914–921. doi: 10.1038/ni.3457
53. Wilhelmsen, K, Litjens, SH, Kuikman, I, Tshimbalanga, N, Janssen, H, van den Bout, I, Raymond, K, Sonnenberg, A. Nesprin-3, a novel outer nuclear membrane protein, associates with the cytoskeletal linker protein plectin. *J Cell Biol.* 2005;171:799–810. doi: 10.1083/jcb.200506083

54. Ketema, M, Wilhelmsen, K, Kuikman, I, Janssen, H, Hodzic, D, Sonnenberg, A. Requirements for the localization of nesprin-3 at the nuclear envelope and its interaction with plectin. *J Cell Sci.* 2007;120:3384–3394. doi: 10.1242/jcs.014191
55. Staszewska, I, Fischer, I, Wiche, G. Plectin isoform 1-dependent nuclear docking of desmin networks affects myonuclear architecture and expression of mechanotransducers. *Hum Mol Genet.* 2015;24:7373–7389. doi: 10.1093/hmg/ddv438
56. Gimpel, P, Lee, YL, Sobota, RM, Calvi, A, Koullourou, V, Patel, R, Mamchaoui, K, Nédélec, F, Shackleton, S, Schmoranzer, J, et al. Nesprin-1 α - dependent microtubule nucleation from the nuclear envelope via Akap450 is necessary for nuclear positioning in muscle cells. *Curr Biol.* 2017;27:2999–3009.e9. doi: 10.1016/j.cub.2017.08.031
57. Ramspacher, C, Steed, E, Boselli, F, Ferreira, R, Faggianelli, N, Roth, S, Spiegelhalter, C, Messaddeq, N, Trinh, L, Liebling, M, et al. Developmental alterations in heart biomechanics and skeletal muscle function in desmin mutants suggest an early pathological root for desminopathies. *Cell Rep.* 2015;11:1564–1576. doi: 10.1016/j.celrep.2015.05.010
58. Ketema, M, Kreft, M, Secades, P, Janssen, H, Sonnenberg, A. Nesprin-3 connects plectin and vimentin to the nuclear envelope of sertoli cells but is not required for sertoli cell function in

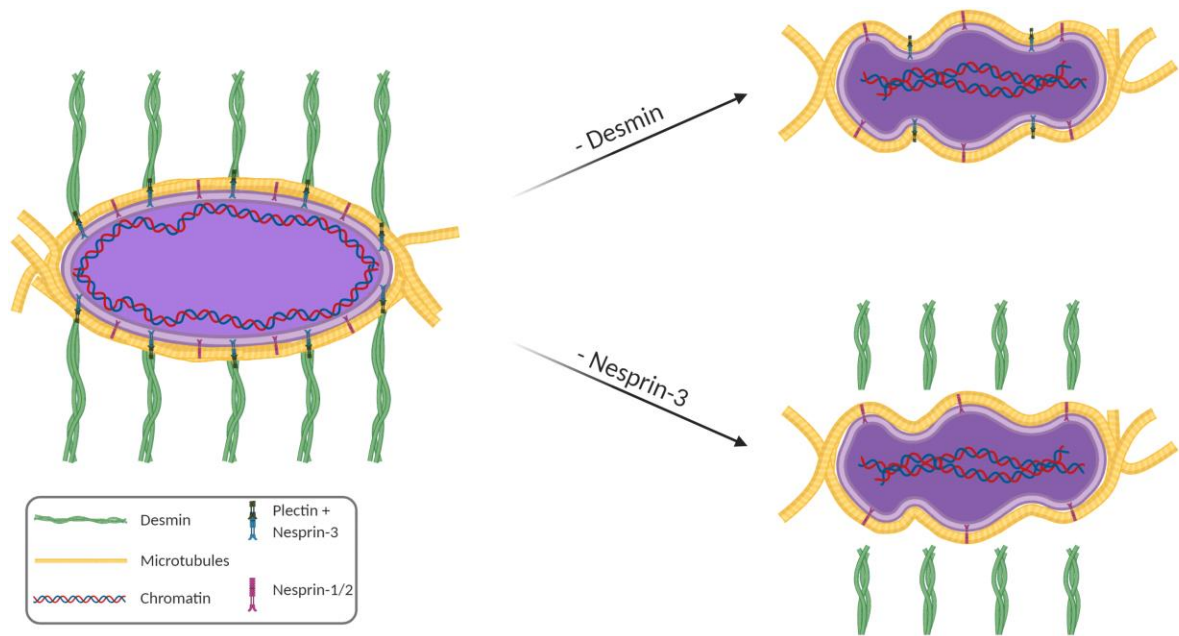
- spermatogenesis. *Mol Biol Cell*. 2013;24:2454–2466. doi: 10.1091/mbc.E13-02-0100
59. Nabet, B., Roberts, JM., Buckley, DL., Paulk, J., Dastjerdi, S., Yang, A., Leggett, AL., Erb, MA., Lawlor, MA., Souza, A., Scott, TG., Vittori, S., Perry, JA., Qi, J., Winter, GE., Wong, K., Gray, NS. and Bradner, JE. The dTAG system for immediate and target-specific protein degradation. *Nature Chemical Biology*. 2018;14:431-441. doi: 10.1038/s41589-018-0021-8
60. Nabet, B., Ferguson, FM., Seong, BKA., Kuljanin, M., Leggett, AL., Mohardt, ML., Robichaud, A., Conway, AS., Buckley, DL., Mancias, JD., Bradner, JE., Stegmaier, K., and Gray, NS. Rapid and direct control of target protein levels with VHL-recruiting dTAG molecules. *Nature Communications*. 2020;11:4687. doi: 10.1038/s41467-020-18377-w
61. Thornell, L, Carlsson, L, Li, Z, Mericskay, M, Paulin, D. Null mutation in the desmin gene gives rise to a cardiomyopathy. *J Mol Cell Cardiol*. 1997;29:2107–2124. doi: 10.1006/jmcc.1997.0446
62. Graziano, S, Kreienkamp, R, Coll-Bonfill, N, Gonzalo, S. Causes and consequences of genomic instability in laminopathies: replication stress and interferon response. *Nucleus*. 2018;9:258–275. doi: 10.1080/19491034.2018.1454168
63. Irianto, J, Xia, Y, Pfeifer, CR, Athirasala, A, Ji, J, Alvey, C, Tewari, M, Bennett, RR, Harding, SM, Liu, AJ, et al. DNA damage follows repair

factor depletion and portends genome variation in cancer cells after pore migration. *Curr Biol.* 2017;27:210–223. doi: 10.1016/j.cub.2016.11.049

64. Yu, T, MacPhail, SH, Banáth, JP, Klovov, D, Olive, PL. Endogenous expression of phosphorylated histone H2AX in tumors in relation to DNA double-strand breaks and genomic instability. *DNA Repair (Amst)*. 2006;5:935–946. doi: 10.1016/j.dnarep.2006.05.040
65. Shah, PP, Donahue, G, Otte, GL, Capell, BC, Nelson, DM, Cao, K, Aggarwala, V, Cruickshanks, HA, Rai, TS, McBryan, T, et al. Lamin B1 depletion in senescent cells triggers large-scale changes in gene expression and the chromatin landscape. *Genes Dev.* 2013;27:1787–1799. doi: 10.1101/gad.223834.113
66. Peric-Hupkes, D, Meuleman, W, Pagie, L, Bruggeman, SW, Solovei, I, Brugman, W, Gräf, S, Flicek, P, Kerkhoven, RM, van Lohuizen, M, et al. Molecular maps of the reorganization of genome-nuclear lamina interactions during differentiation. *Mol Cell.* 2010;38:603–613. doi: 10.1016/j.molcel.2010.03.016
67. Salomon, A., Okami, N., Heffler, J., Robison, P., Bogush, A. and Prosser, BL. In Preparation. 2021.
68. Kohwi, M, Lupton, JR, Lai, SL, Miller, MR, Doe, CQ. Developmentally regulated subnuclear genome reorganization restricts neural progenitor competence in *Drosophila*. *Cell.* 2013;152:97–108. doi: 10.1016/j.cell.2012.11.049

69. Swift, J, Ivanovska, IL, Buxboim, A, Harada, T, Dingal, PC, Pinter, J, Pajerowski, JD, Spinler, KR, Shin, JW, Tewari, M, et al. Nuclear lamin-A scales with tissue stiffness and enhances matrix-directed differentiation. *Science*. 2013;341:1240104. doi: 10.1126/science.1240104
70. Guilluy, C, Osborne, LD, Van Landeghem, L, Sharek, L, Superfine, R, Garcia-Mata, R, Burrridge, K. Isolated nuclei adapt to force and reveal a mechanotransduction pathway in the nucleus. *Nat Cell Biol*. 2014;16:376–381. doi: 10.1038/ncb2927
71. Cho, S, Vashisth, M, Abbas, A, Majkut, S, Vogel, K, Xia, Y, Ivanovska, IL, Irianto, J, Tewari, M, Zhu, K, et al. Mechanosensing by the lamina protects against nuclear rupture, DNA damage, and cell- cycle arrest. *Dev Cell*. 2019;49:920–935.e5. doi: 10.1016/j.devcel.2019.04.020
72. Shah, SB, Davis, J, Weisleder, N, Kostavassili, I, McCulloch, AD, Ralston, E, Capetanaki, Y, Lieber, RL. Structural and functional roles of desmin in mouse skeletal muscle during passive deformation. *Biophys J*. 2004;86:2993–3008. doi: 10.1016/S0006-3495(04)74349-0
73. Milner, DJ, Taffet, GE, Wang, X, Pham, T, Tamura, T, Hartley, C, Gerdes, AM, Capetanaki, Y. The absence of desmin leads to cardiomyocyte hypertrophy and cardiac dilation with compromised systolic function. *J Mol Cell Cardiol*. 1999;31:2063–2076. doi: 10.1006/jmcc.1999.1037

74. Li, M, Andersson-Lendahl, M, Sejersen, T, Arner, A. Knockdown of desmin in zebrafish larvae affects interfilament spacing and mechanical properties of skeletal muscle. *J Gen Physiol.* 2013;141:335–345. doi: 10.1085/jgp.201210915
75. Heling, A, Zimmermann, R, Kostin, S, Maeno, Y, Hein, S, Devaux, B, Bauer, E, Klövekorn, WP, Schlepper, M, Schaper, W, et al. Increased expression of cytoskeletal, linkage, and extracellular proteins in failing human myocardium. *Circ Res.* 2000;86:846–853. doi: 10.1161/01.res.86.8.846
76. Nikolova, V, Leimena, C, McMahon, AC, Tan, JC, Chandar, S, Jogia, D, Kesteven, SH, Michalicek, J, Otway, R, Verheyen, F, et al. Defects in nuclear structure and function promote dilated cardiomyopathy in lamin A/C-deficient mice. *J Clin Invest.* 2004;113:357–369. doi: 10.1172/JCI19448
77. Roman, W, Martins, JP, Carvalho, FA, Voituriez, R, Abella, JVG, Santos, NC, Cadot, B, Way, M, Gomes, ER. Myofibril contraction and crosslinking drive nuclear movement to the periphery of skeletal muscle. *Nat Cell Biol.* 2017;19:1189–1201. doi: 10.1038/ncb3605
78. Heffler, J., Shah, PP., Robison, P., Phyo, S., Veliz, K., Uchida, K., Bogush, A., Rhoades, J., Jain, R. and Prosser, BL. A Balance Between Intermediate Filaments and Microtubules Maintains Nuclear Architecture in the Cardiomyocyte. *Circulation Research.* 2019;126:e10-e26. doi: 10.1161/CIRCRESAHA.119.315582Ci



Graphical Abstract: Desmin and microtubules work in concert to maintain nuclear homeostasis and chromatin organization. Desmin (light green filaments) attached to the nucleus via plectin (dark green linker) and nesprin-3 (light blue linker). Due to desmin's attachments to the intermediate filament, myofibril, and microtubule network, this connection links the nucleus to the surrounding cytoskeleton. Moreover, desmin itself and through binding partners, associates with diverse cellular structures such as the mitochondria, intercalated disc, z-disc, costameres and sarcolemma, attaching the nucleus directly to these components. We hypothesize this attachment provides a robust tension on the nucleus, providing structural integrity to the lamina and maintaining homeostatic signal transduction via the LINC attachment to the lamina. Complementarily, the microtubules (gold), attach to nesprin-1/2 (pink linker). This perinuclear location serves as a nucleation site and likely an important post-transcriptional, post-export site for mRNA. In the absence of the desmin-nesprin-3 axis, microtubule growth around the nucleus causes deformation. This causes malformations in the nuclear lamina, disruption of chromatin (red and blue DNA structure) and its organization, and loss of nuclear homeostasis.

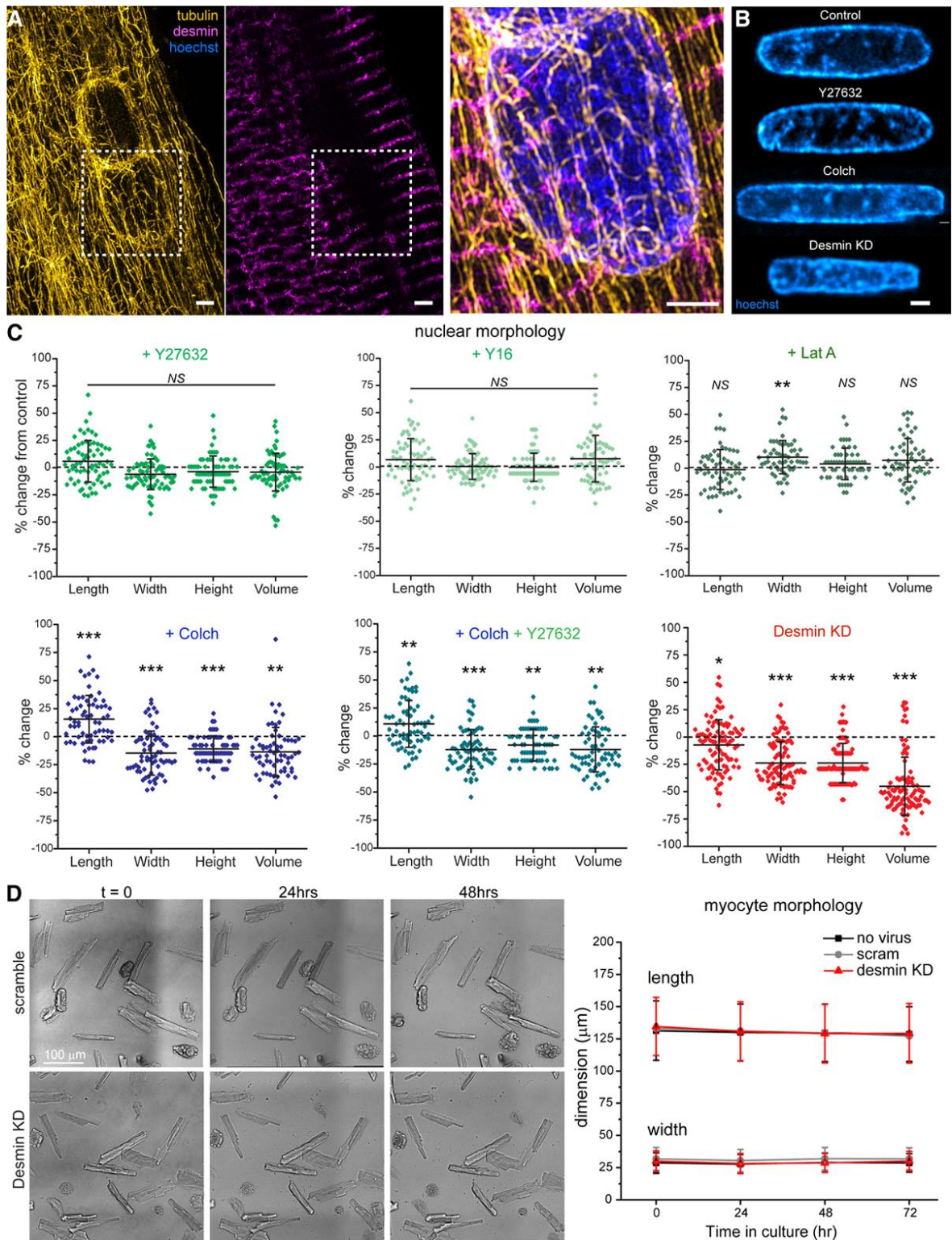


Figure 1: Acute desmin depletion causes involution of cardiomyocyte nuclei. A, Structured illumination microscopy (SIM) image showing the close association between microtubules

(yellow), desmin (magenta), and the nucleus (blue). **Right** shows zoom merge from dotted box. Scale bar =1 μm . **B**, Representative Hoechst-stained live adult rat CM nuclei. **C**, Nuclear size parameters represented by percent change from time-matched control mean. Dimethyl sulfoxide (DMSO; Y27632): N=3 hearts, n=68 nuclei; Y27632 (10 $\mu\text{mol/L}$ 24 h): N=3, n=69; Y16 (10 $\mu\text{mol/L}$ 24 h): N=3, n=66; DMSO (LatA): N=3, n=58; LatA (10 $\mu\text{mol/L}$ 24 h): N=3, n=56; DMSO (colchicine [colch]): N=3, n=82; colch (1 $\mu\text{mol/L}$ for 24 h): N=3, n=81; Y27632 (10 $\mu\text{mol/L}$ 24 h) + colch (1 $\mu\text{mol/L}$ 24 h): N=3, n=67; scramble (48 h): N=3, n=85, Desmin knockdown (KD; 48 h): N=3, n=98. Statistical significance determined via 1-way ANOVA with post hoc Bonferroni correction. **D**, Transmitted light images (**left**) of identical cardiomyocytes at different time points in culture; quantification (**right**) of cardiomyocyte length and width over time in culture. No virus N=2, n=157, scram N=2, n=138, desmin KD N=2, n=128. Data presented as mean \pm 1 SD. For statistical significance, * P <0.05, ** P <0.01, *** P <0.001 vs control

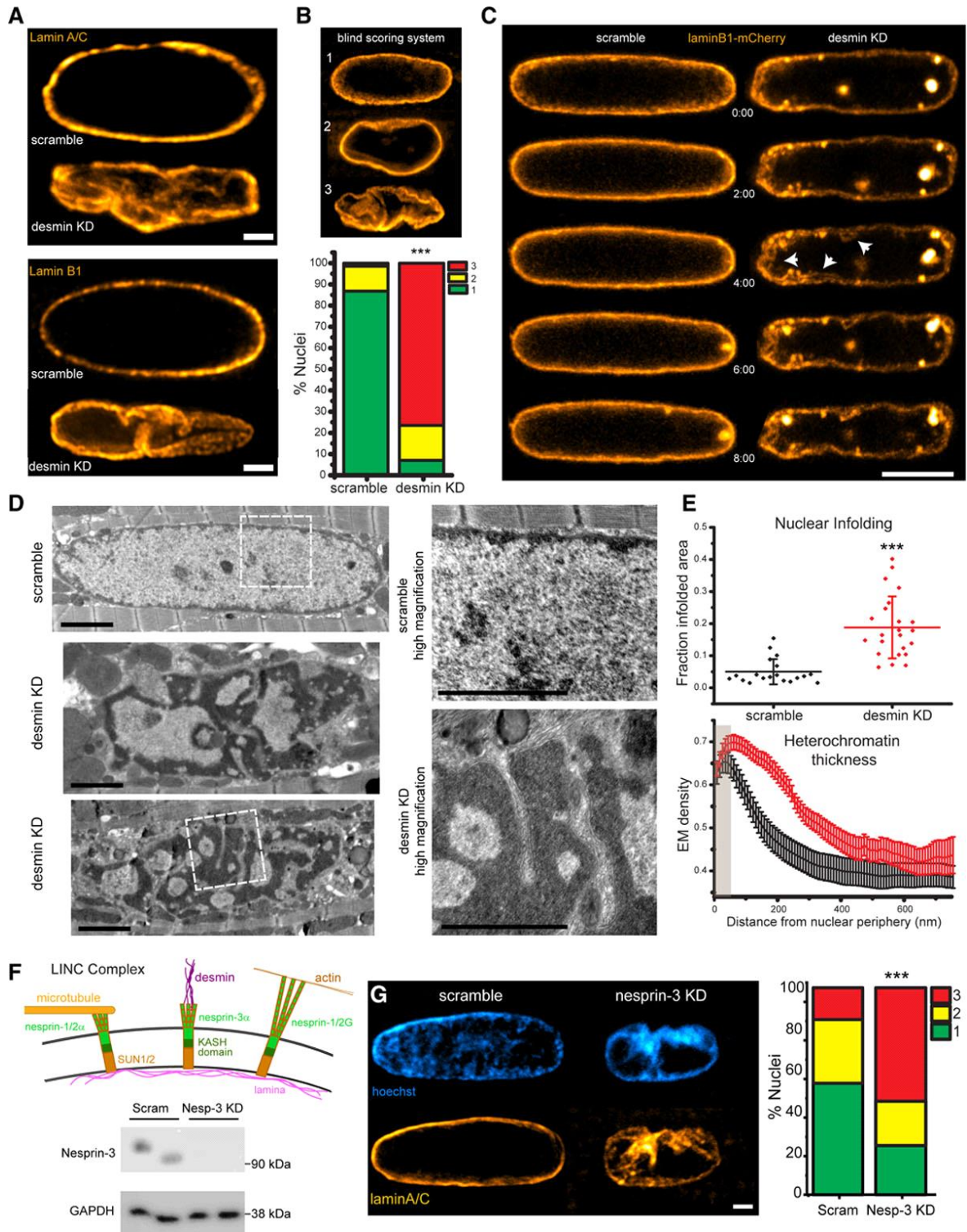
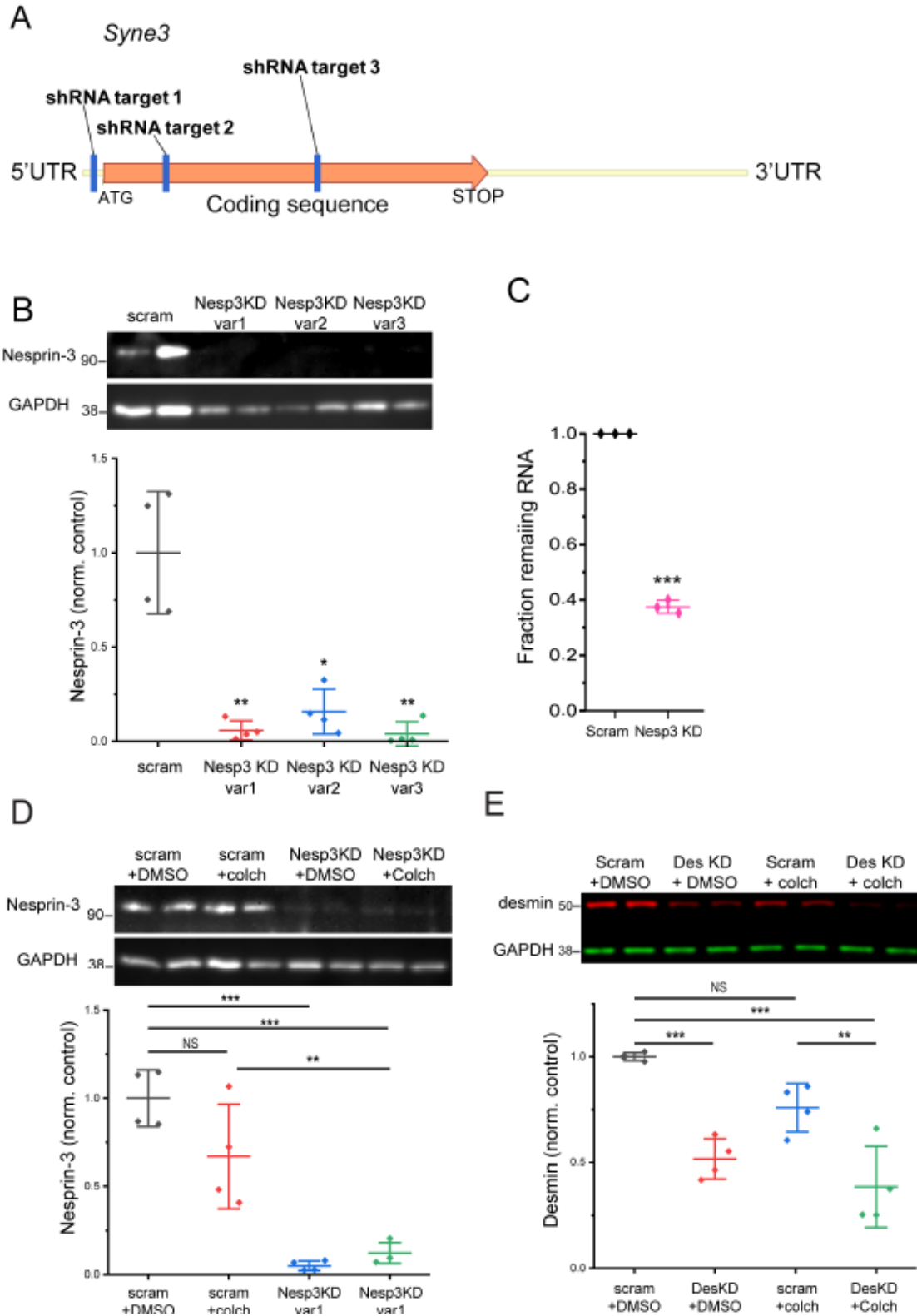


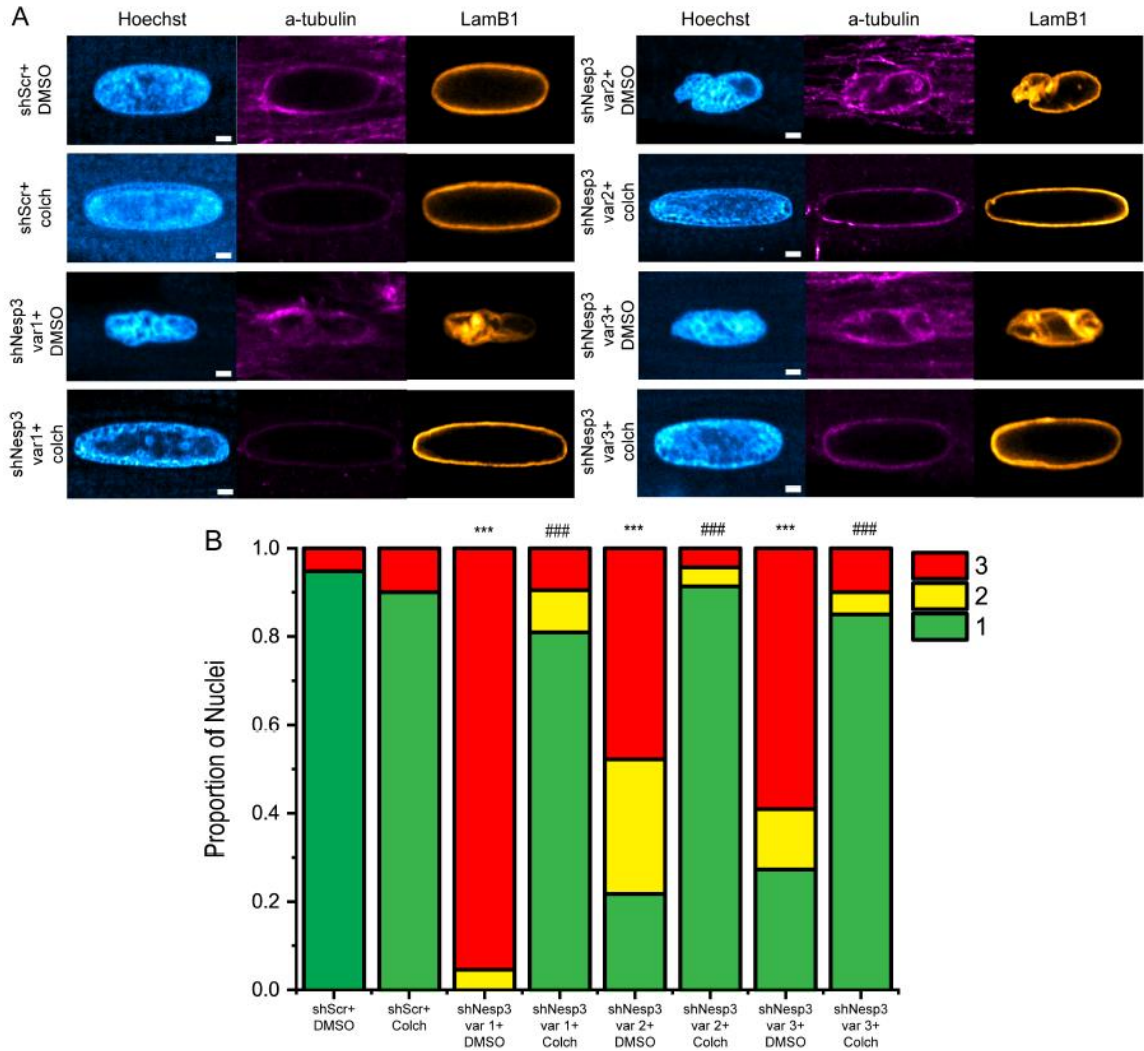
Figure 2: Acute desmin or nesprin (nuclear envelope spectrin repeat protein)-3 depletion causes lamina infolding. A, Representative lamin A/C (upper) or lamin B1 (lower)

immunostaining in cardiomyocyte nuclei upon scramble or desmin knockdown (KD). Scale=1 μm . **B**, Grading scale developed to assess the severity of lamina defects. **Upper** shows examples of 1 or nearly perfect nuclei (≤ 1 -fold or malformation), 2 or nuclei with mild defects (2- to 3-folds or malformations), and 3 or highly disrupted lamina architecture (3+ folds or malformations). **Lower** shows the result of blinded grading as represented by percent nuclei. Control (48 h scramble): N=3, n=68. Desmin KD (48 h): N=3, n=85. Statistical significance determined using χ^2 test. **C**, Time-lapse images of cardiomyocytes coinfecting with lamin B1-mCherry and scramble (**left**) or desmin KD (**right**) starting at ≈ 30 h post-infection. White arrows emphasize discrete regions of lamina infolding. **D**, Electron microscopy representative images of nuclei from longitudinal sections of either scramble (**top**) or desmin KD (**middle** and **bottom**) cardiomyocytes. The **right** shows higher magnification images of the boxed regions at left. **Left**: scale = 2 μm . **Right**: scale = 200 nm. **E**, **Upper** shows quantification of the fraction of infolded area per nucleus. **Lower** shows quantification of the proliferation of electron-dense material (interpreted as heterochromatin) and its distance dependence tangential to the nuclear envelope. Gray bar on the left denotes the uncertainty in the precise location of the inner nuclear membrane due to the resolution limit. scramble: N=2, n=18. Desmin KD: N=2, n=23. Statistical significance determined using 2-sided *t* test. Line graph represents the mean with whiskers representing the SE. **F**, **Top**, cartoon schematic of the cardiomyocyte linkers of the nucleoskeleton and cytoskeleton (LINC) complex. **Bottom**, Western blot showing nesprin-3 KD in response to shRNA-mediated KD using variant 1. Quantification can be found in Online Figure IIB. **G**, Immunofluorescence (**left**) of Hoechst and lamin B1 in CM nuclei 48 h after infection with scramble or shNesprin-3 variant 1. Scale = 1 μm . Nuclear grading (**right**) of nesprin-3 KD nuclei. scramble: N=2, n=39. Nesprin-3 KD: N=2, n=31. Statistical significance determined via χ^2 test. For statistical significance, **P*<0.05, ***P*<0.01, ****P*<0.001 vs control.



Supplemental Figure 2: Multiple nesprin-3 shRNA variants are able decrease nesprin-3 levels. A, Schematic of shRNA targeting sites on SYNE3, the gene encoding nesprin-3. **B**,

Western blot (**upper**) and quantification (**lower**) confirming robust nesprin-3 depletion by three separate oligos. Statistical significance determined by two-way ANOVA with Bonferroni correction. **C**, Fraction remaining nesprin-3 mRNA (2-ddCt), determined via qRT-PCR after shRNA-mediated KD using variant 1. Primers detecting nesprin-3 lie between exons 17 and 18 and will detect both splice forms of nesprin-3. Statistical significance determined using two-sided t-test. **D**, Western blot (**upper**) and quantification (**lower**) confirming robust nesprin3 depletion is unaltered upon colchicine treatment from experiment described in Fig 3B. Statistical significance determined by two-way ANOVA with Bonferroni correction. **E**, Western blot (**upper**) and quantification (**lower**) confirming robust desmin depletion is unaltered upon colchicine treatment from experiment described in Fig 3B. Statistical significance determined by two-way ANOVA with Bonferroni correction. For all box plots, the middle line represents the mean, and the whiskers indicate 1 SD from the mean.



Supplemental Figure 3: Multiple nesprin-3 shRNA variants cause nuclear infolding in a microtubule-dependent manner. **A**, Immunofluorescence of nuclei treated with the different nesprin-3 shRNA variants showing DNA (Hoechst), a-tubulin (magenta) and lamin B1 (orange). Nuclear involution and lamina infolding that are rescued with colchicine. Scale bar = 2 μ m. **B**, Blinded nuclear grading of nuclei from Supp Fig 2D. shScrambled (48 hrs) + DMSO: N=2 rats, n=19 nuclei. shScrambled (48 hrs) + Colch (10 μ M 30 hrs): N=2, n=20. shNesp3 var1 (48 hrs) + DMSO: N=2, n=22. shNesp3 var1 (48 hrs) + Colch (10 μ M 30 hrs): N=2, n=21. shNesp3 var2 (48 hrs) + DMSO: N=2, n=23. shNesp3 var2 (48 hrs) + Colch (10 μ M 30 hrs): N=2, n=23. shNesp3 var3 (48 hrs) + DMSO: N=2, n=22. shNesp3 var3 (48 hrs) + Colch (10 μ M 30 hrs): N=2, n=20. *= p-value vs shScrambled + DMSO. #= vs shNesp3 + DMSO. Statistical significance determined

via chi-square. For statistical significance, * = $p < 0.05$, ** = $p < 0.01$, *** = $p < 0.001$ vs. control; # = $p < 0.05$, ## = $p < 0.01$, ### = $p < 0.001$ vs. desmin KD + DMSO or nesprin KD + DMSO.

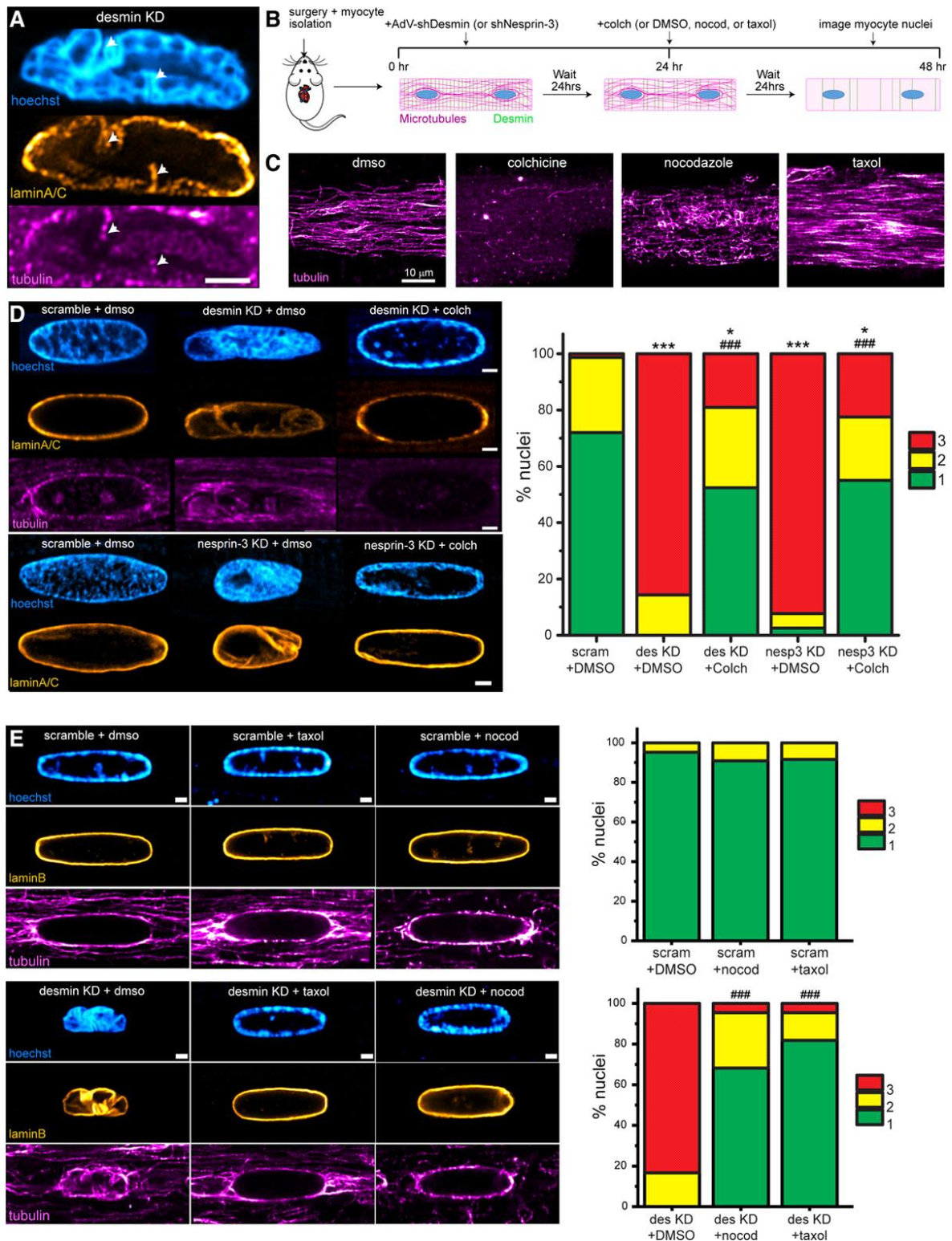
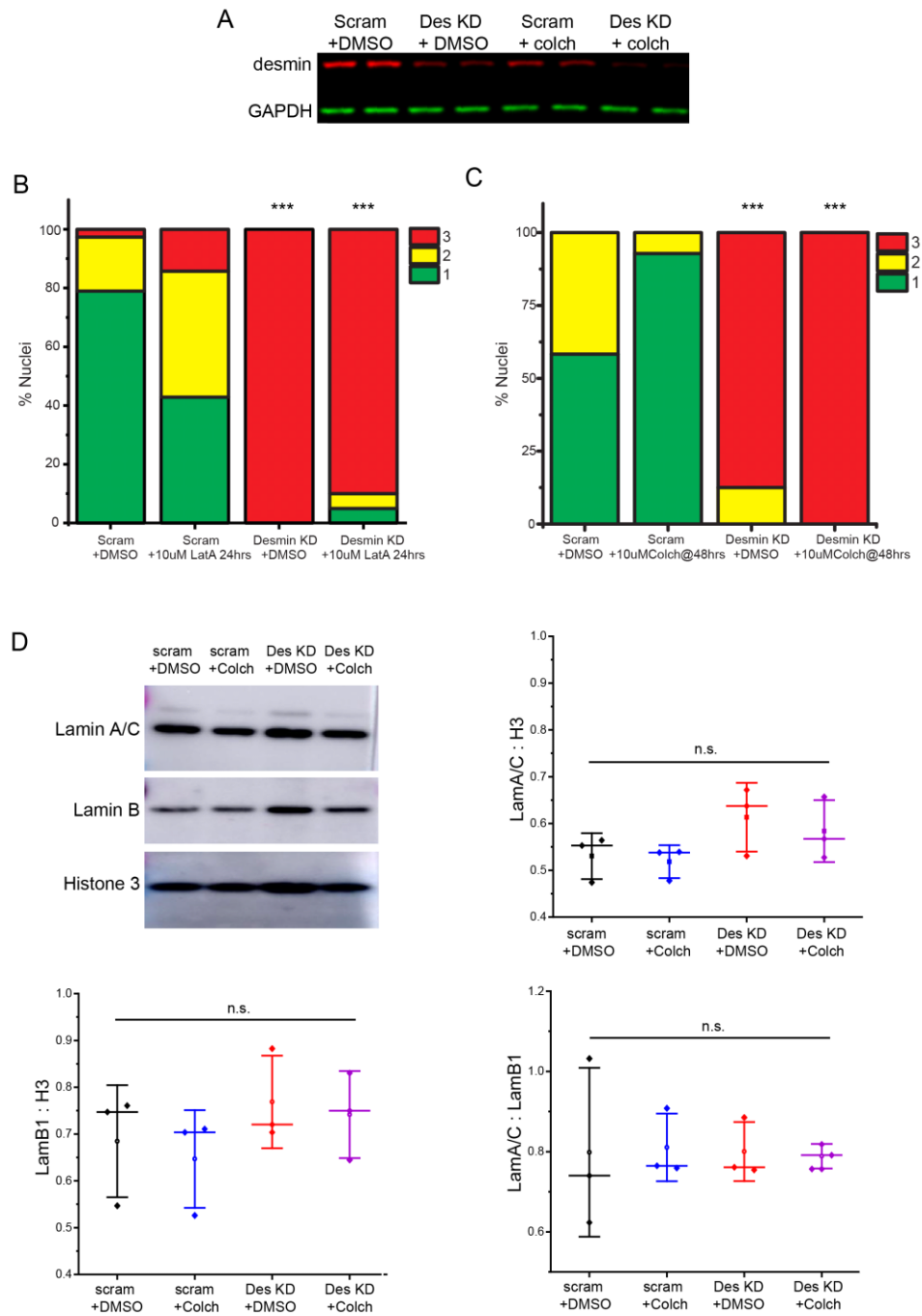


Figure 3: Disrupting dynamic microtubules prevents nuclear defects arising from desmin or nesprin (nuclear envelope spectrin repeat protein)-3 depletion. A, Representative image

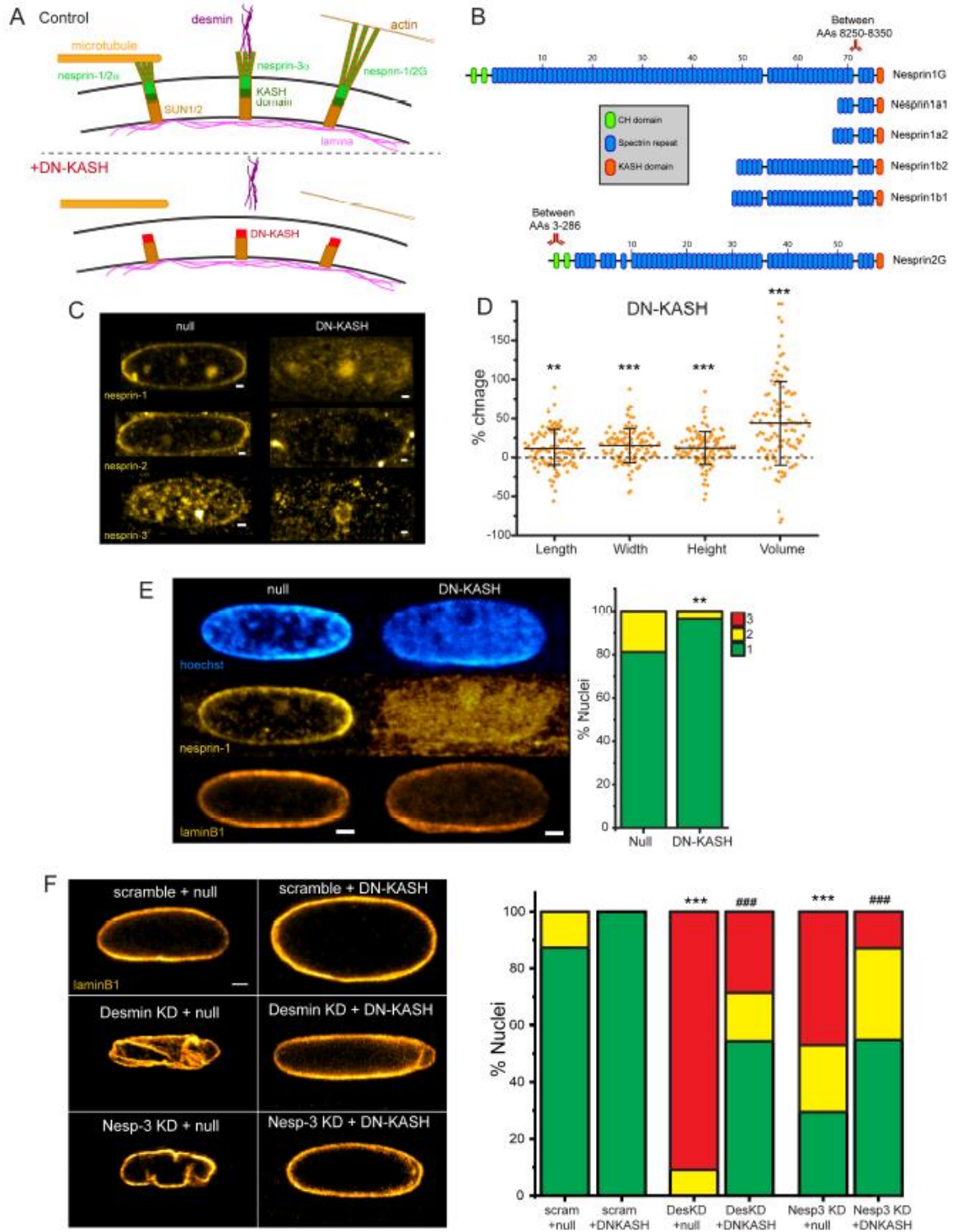
of desmin knockdown (KD) nucleus displaying microtubules present in nuclear infolds (white arrows). Scale =2 μm . **B**, Experimental schematic for microtubule and desmin disruption. **C**, Representative images of microtubules in cardiomyocytes following treatment with microtubule-targeting drugs. **D**, Representative images (**left**) of nuclei from experiment depicted in **B**. Scale bar is 1 μm . Blinded nuclear grading (**right**) of nuclei. scramble + dimethyl sulfoxide (DMSO): N=2, n=38. Desmin KD + DMSO: N=2, n=28. Desmin KD + colchicine (colch; 10 $\mu\text{mol/L}$): N=2, n=42. Nesprin-3 KD + DMSO: N=2, n=39. Nesprin-3 KD + colch (10 $\mu\text{mol/L}$): N=2, n=40. Statistical significance determined via χ^2 test. **E**, Representative images (**left**) and nuclear grading (**right**) from experiment depicted in **B**. Scale bar is 2 μm . Scramble + DMSO: N=2, n=21. Scramble + nocodazole (0.5 $\mu\text{mol/L}$): N=2, n=22. Scramble + taxol (10 $\mu\text{mol/L}$): N=2, n= 24. Desmin KD + DMSO: N=2, n=24. Desmin KD + nocodazole (0.5 $\mu\text{mol/L}$): N=2, n=22. Desmin KD + taxol (10 $\mu\text{mol/L}$): N=2, n=22. Statistical significance determined via χ^2 test. For statistical significance, * P <0.05, ** P <0.01, *** P <0.001 vs control; # P <0.05, ## P <0.01, ### P <0.001 vs desmin KD + DMSO or nesprin-3 KD + DMSO.



Supplemental Figure 4: Nuclear infolding is irreversible but is not associated with changes

to Lamin A/B1/C levels. **A**, Western blot showing desmin (red) and GAPDH (green). Cells were treated with either shScrambled or Des KD AdV and either DMSO or Colchicine. **B**, Blinded nuclear grading of desmin KD- and LatA-treated nuclei. LatA treatment was timed to disrupt actin

prior to infold formation. shScrambled (48 hrs) + DMSO: N=3 rats, n=38 nuclei. shScrambled (48 hrs) + LatA (10 μ M 24hrs): N=1, n=7. Desmin KD (48 hrs) + DMSO: N=1, n=20. Desmin KD (48 hrs) + LatA (10 μ M 24hrs): N=1, n=20. * = p-value vs shScrambled + DMSO. # = vs Desmin KD + LatA. Statistical significance determined via One-Way ANOVA with Bonferroni correction. **C**, Blinded nuclear grading of desmin KD- and colchicine-treated nuclei. Colch treatment was timed to disrupt microtubules after infold information. **D**, Representative western blot showing Lamin A/C, Lamin B1, and Histone 3 (H3), and blot quantification, normalized to H3. Each data point represents one biological repeat. For all box plots, the middle line represents the mean, and the whiskers indicate 1 SD from the mean. For statistical significance, * = $p < 0.05$, ** = $p < 0.01$, *** = $p < 0.001$ vs. control.



Supplemental Figure 5: DN-KASH causes nuclear swelling, rescues desmin and nesprin-3

KD. Disrupting the LINC complex prevents nuclear involution. **A**, Cartoon schematic of the cardiomyocyte LINC complex and effect of DN-KASH. **B**, Schematic of different nesprin-1 splice forms and binding sites of nesprin-1 and nesprin-2G antibodies. **C**, Immunofluorescence of

nesprins 1-3 in null or DN-KASH expressing cardiomyocytes. Scale = 1 μ m. **D**, Nuclear size parameters presented as percent change from paired control mean. Null: N= 3, n= 65. DN KASH: N= 3, n= 107. **E**, Immunofluorescence (left) of Hoechst, nesprin-1 and laminB1 in either null or DN-KASH expressing cardiomyocytes. Scale = 1 μ m. Blinded nuclear grading (**right**) of DN-KASH nuclei. Null: N= 3, n= 64. DN KASH: N= 3, n= 58. Statistical significance determined via Chi-squared test. **F**, Immunofluorescence (**left**) of LaminB1 in myocytes co-transduced with Scramble/Des KD/Nesp-3 KD and Null/DN-KASH encoding adenoviruses. Nuclear grading (**right**) of DN-KASH rescue experiments. Scram + null: N=4, n=63; scram + DNKASH: N=4, n=67; des KD + null: N=2, n=33; des KD + DNKASH: N=2, n=35; nesp3KD+null: N=2, n=34; nesp3KD+DNKASH: N=2, n=31. Statistical significance determined via Chi-squared test. For statistical significance, * = $p < 0.05$, ** = $p < 0.01$, *** = $p < 0.001$ vs. control; # = $p < 0.05$, ## = $p < 0.01$, ### = $p < 0.001$ vs. desmin KD + null or nesprin-3 KD + null.

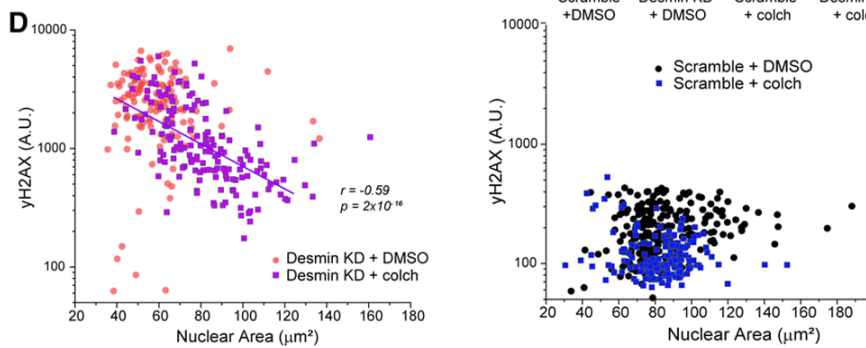
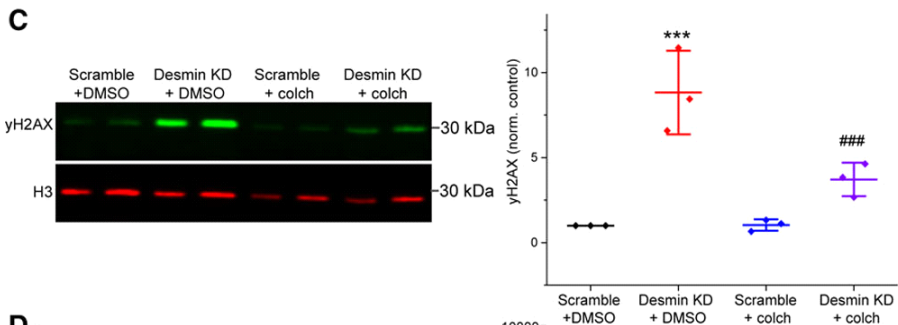
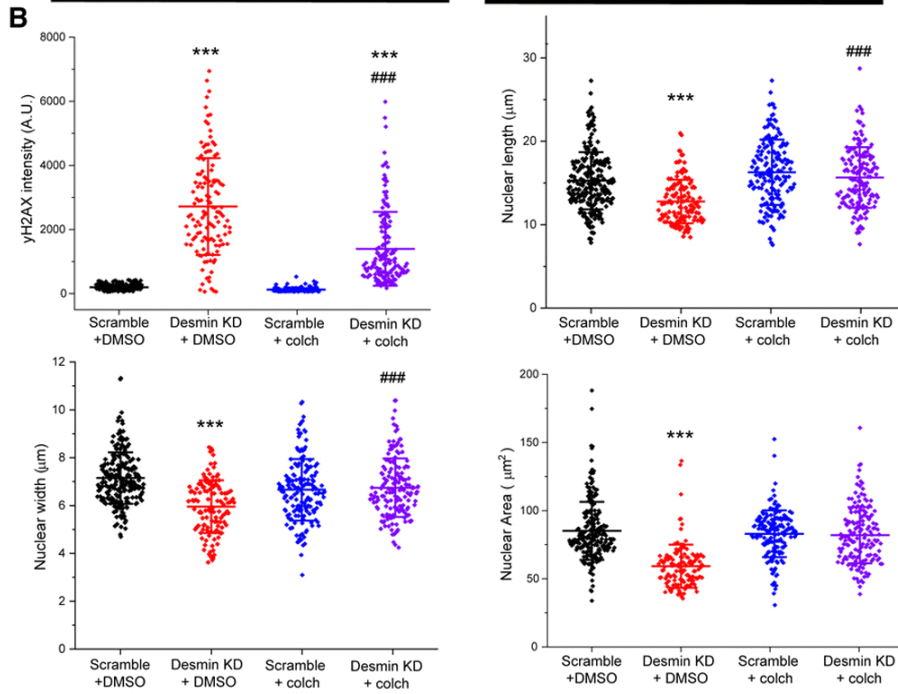
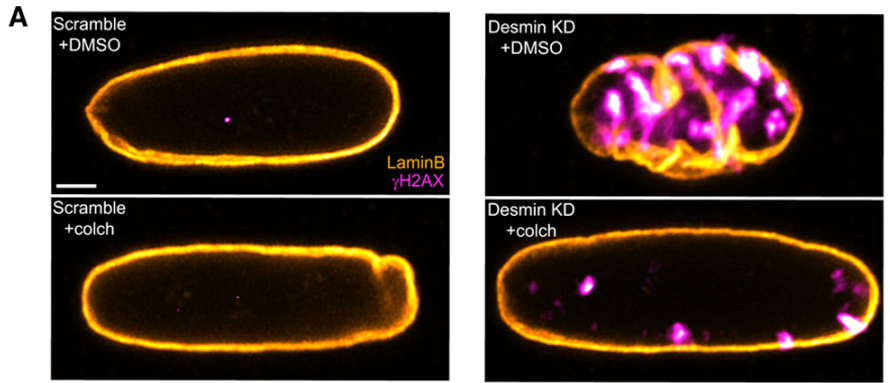


Figure 4: Desmin knockdown (KD) causes DNA damage that is partially prevented by microtubule depolymerization. **A**, Representative immunofluorescence images of γ H2AX, an indicator of DNA damage and repair. **B**, γ H2AX intensity, nuclear length, width, and area measured from immunofluorescence imaging. Scrambled (48 h) + dimethyl sulfoxide (DMSO): N=2, n=226. Desmin KD (48 h) + DMSO N=2, n=128. Scrambled (48 h) + colchicine (colch; 10 μ mol/L 32 h): N=2, n=157. Desmin KD (48 h) + colch (10 μ mol/L 32 h): N=2, n=160. **C**, Western blot (left) and quantification (right) for γ H2AX (green) and H3 (red, loading control). Treatment conditions are identical as above. Repeat lanes in each group are 5 and 7 μ L of lysate, and the quantification always pulled from the average of 5 and 7 μ L of lysate and normalized to H3. Data are from 3 independent rat CM isolations. H3 is unaltered with either desmin KD or colch treatment (data not shown). Statistical significance determined via 2-way ANOVA with post hoc Bonferroni. **D**, Correlation between γ H2AX and nuclear area from the same experiments. γ H2AX signal was plotted on a logarithmic axis to demonstrate the exponential relationship between nuclear area and DNA damage, and so that the distribution of scramble data could be visualized on the same scale. Log10 transformed data for desmin KD + colch group was fit to linear regression analysis, with the Pearson correlation coefficient listed and P value indicating that slope is significantly different than zero. For statistical significance, *P<0.05, **P<0.01, ***P<0.001 vs control; #P<0.05, ##P<0.01, ###P<0.001 vs desmin KD + DMSO or nesprin (nuclear envelope spectrin repeat protein)-3 KD + DMSO.

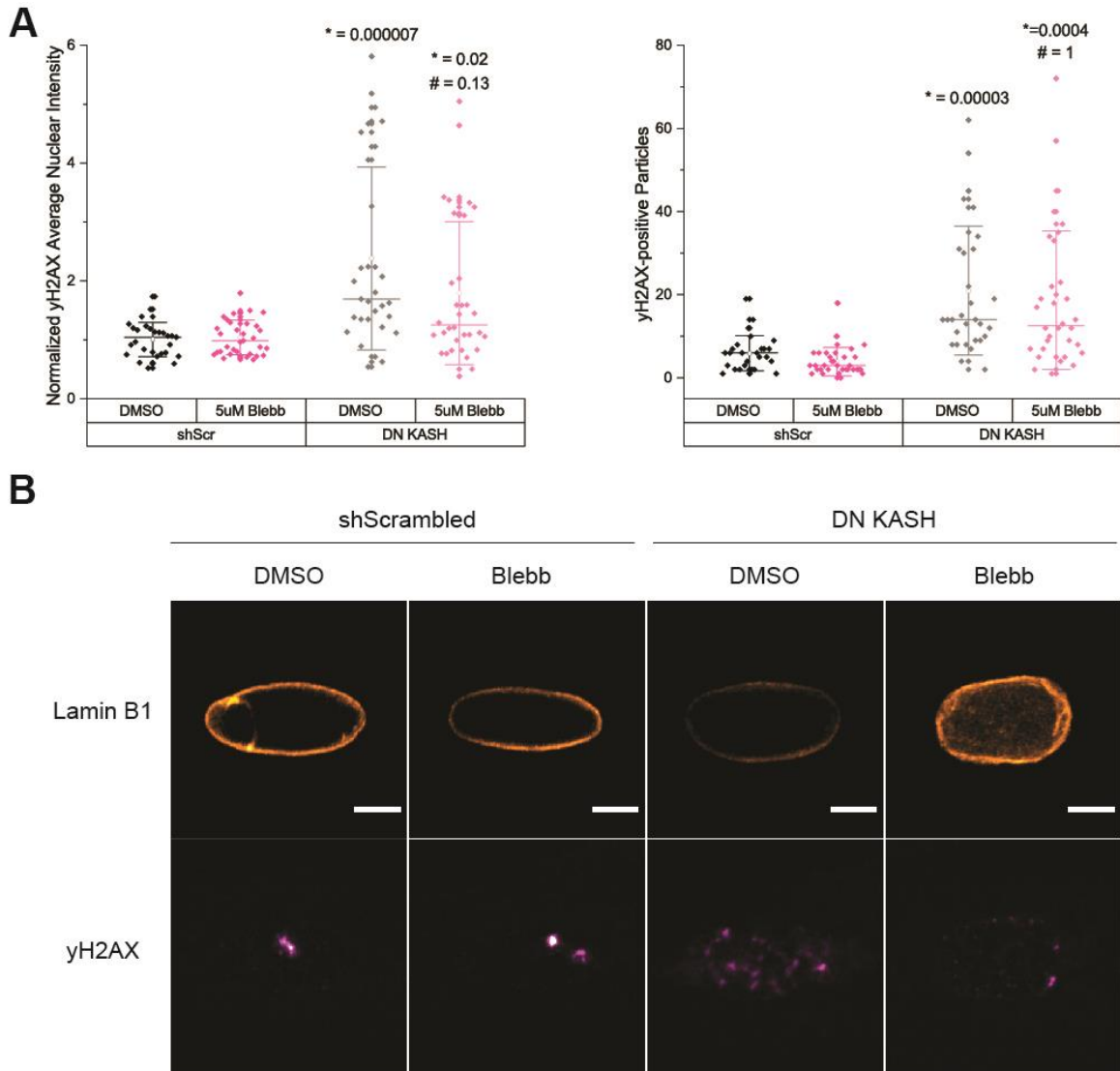


Figure 5: DN KASH causes elevated γ H2AX in adult rat cardiomyocytes. A, Left, Normalized to shScr DMSO control signal intensity average. DN KASH and 5 μ M blebbistatin were incubated for 72 hrs. **Right**, γ H2AX particle counts. Particle number was determined via blinded thresholding and particle analysis. ShScr + DMSO: N= 3 rats, n= 27 nuclei. ShScr + Blebb: N= 3, n= 33. DN KASH + DMSO: N= 3, n= 31. DN KASH + Blebb: N= 3, n= 36. Statistical analysis was conducted using a two-way ANOVA with Bonferroni correction. * represents p-values vs shScr DMSO and # represents p-values vs DN KASH DMSO. **B**, Representative images showing the increase in γ H2AX with DN KASH and the trend toward signal reduction with blebbistatin.

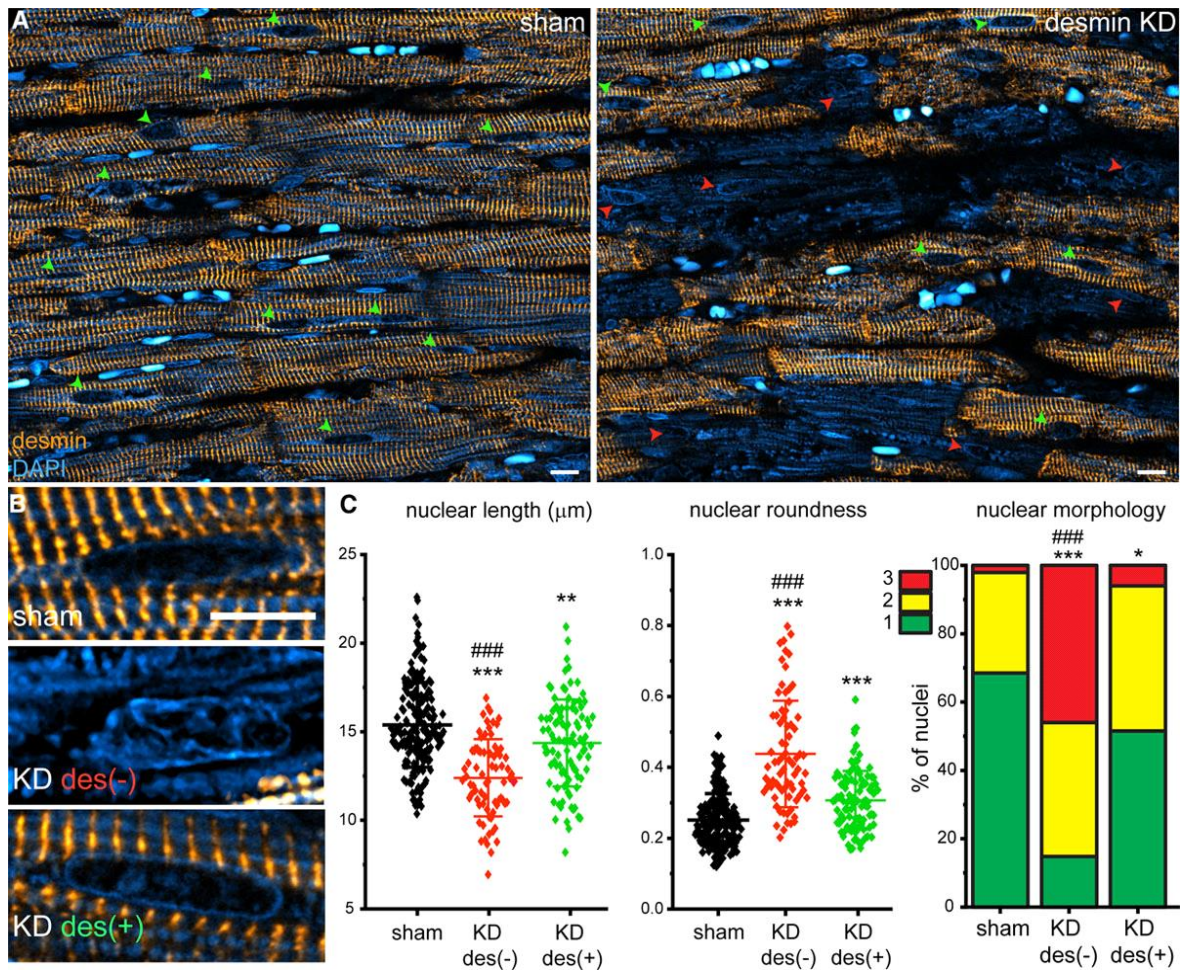


Figure 6: Desmin knockdown (KD) causes nuclear malformation in vivo. **A**, Sham (left) or desmin KD (right) rat left ventricular sections stained with desmin (orange) and DAPI (4',6-diamidino-2-phenylindole; blue). The extranuclear blue signal is background fluorescence in the DAPI channel. Green and red arrows point to desmin-positive and desmin-negative cardiomyocyte nuclei, respectively. Scale =10 µm. Cardiomyocyte nuclei were distinguished from nonmyocyte nuclei via cTNT (cardiac troponin T) counterstaining (not shown). **B**, Zoomed-in images of representative desmin-positive and desmin-negative nuclei in tissue. Scale =1 µm. **C**, Nuclear length (left), roundness (middle), and nuclear grading (right) of nuclei in tissue. *compared to sham, #compared to desmin+ cardiomyocytes. Sham: N=6 hearts, n=188 nuclei. Desmin KD (desmin+): N=4, n=75. Desmin KD (desmin-): N=4, n=100. Statistical significance determined via 1-way ANOVA with post hoc Bonferroni correction for length and roundness and

via χ^2 test for blinded scoring. For statistical significance, * $P < 0.05$, ** $P < 0.01$, *** $P < 0.001$;
$P < 0.05$, ## $P < 0.01$, ### $P < 0.001$.

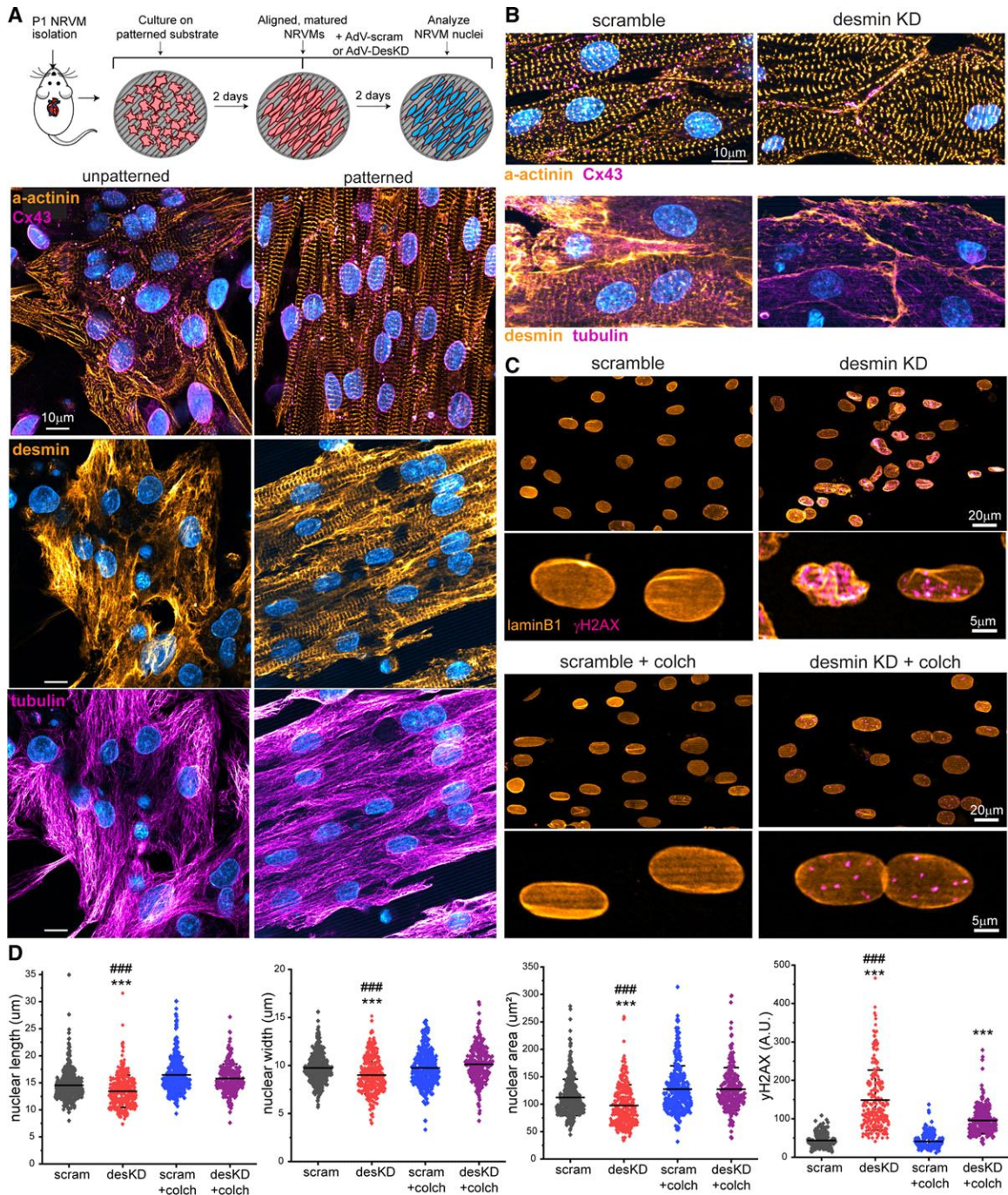


Figure 7: Desmin protects from microtubule-dependent nuclear disruption in beating cardiac syncytia. **A, Top**, experimental design for nanopatterning cardiac syncytia. **Bottom**, immunostaining of a-actinin, desmin, and tubulin in unpatterned (**left**) and patterned (**right**) neonatal rat ventricular myocyte (NRVM) syncytia. Scale = 10 μ m. **B**, Immunostaining of patterned NRVM syncytia in scramble or desmin knockdown (KD) infected cultures. Transverse desmin

filaments are no longer evident upon desmin KD. **C**, Representative field of NRVM nuclei in nanopatterned syncytia immunostained for lamin B1 and γ H2AX (**top**) and 4x zoom in of representative nuclei (**bottom** inset). **D**, Quantification of nuclear dimensions and γ H2AX intensity in NRVM nuclei from nanopatterned syncytia. Scram: N=3 NRVM isolations, n=419 nuclei. Desmin KD: N=3, n=388. Scramble + colchicine (colch): N=3, n=357. Desmin KD + colch: N=3, n= 260. α -actinin (not shown) was used to distinguish myocytes from nonmyocytes. Statistical significance determined via 2-way ANOVA with post hoc Bonferroni comparison. For statistical significance, * P <0.05, ** P <0.01, *** P <0.001 vs control; # P <0.05, ## P <0.01, ### P <0.001 vs desmin KD + dimethyl sulfoxide (DMSO).

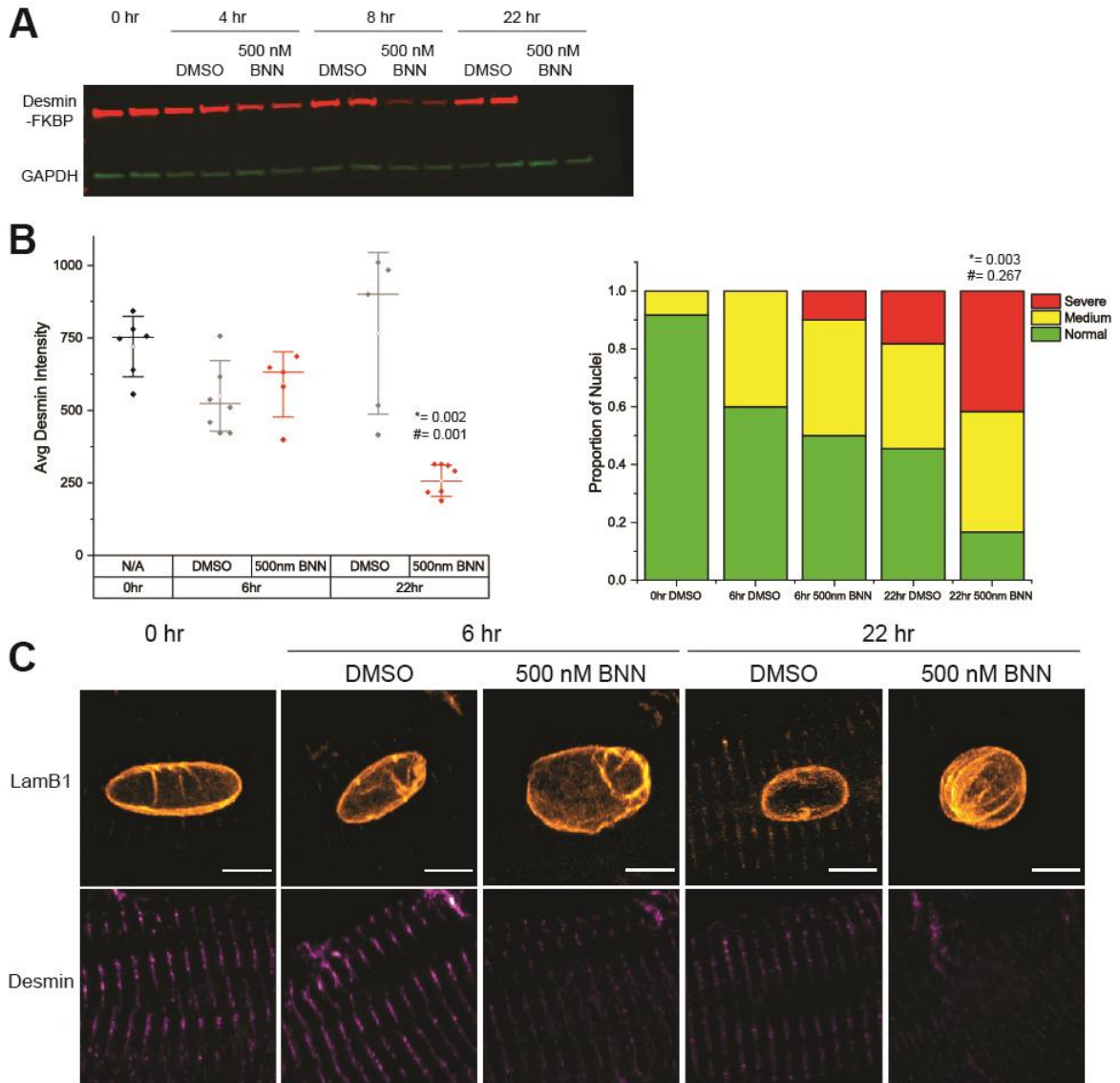


Figure 8: dTAG Desmin degron system causes efficient desmin degradation and nuclear abnormalities. **A**, Western blot showing an adult male homozygous knock-in mouse with desmin-FKBP^{F36V} (red) and GAPDH (green). Cells were treated post isolation with either DMSO or 500 nM dTAGv1 (BNN). BNN causes the desmin chimera to be targeted for degradation with 98 percent of the protein level gone by 22 hrs. **B, Left**, Quantification of the immunofluorescence shown in C. Desmin intensity was determined by blinding the images and picking 3 regions of interest then averaging per cell (each dot is the average for 1 cell). **Right**, Blinded grading of image set as previously described. 0hr: N= 1 rat, n= 12 nuclei. 6hr + DMSO: N= 1, n= 10. 6hr + 500 nM BNN: N= 1, n= 10. 22 hr + DMSO: N= 1, n= 11. 22 hr + 500 nM BNN: N= 1, n= 12. *

refers to p-values compared vs 0 hr control, # refers to p-values vs 22 hr DMSO. **C**,
Representative images showing the changes to the nuclear shape with decreasing desmin and
the decrease in desmin striations over time with BNN. The remaining sign at 22 hr + BNN
appears to be localized to the intercalated disc, the most desmin-rich structure in the
cardiomyocyte.

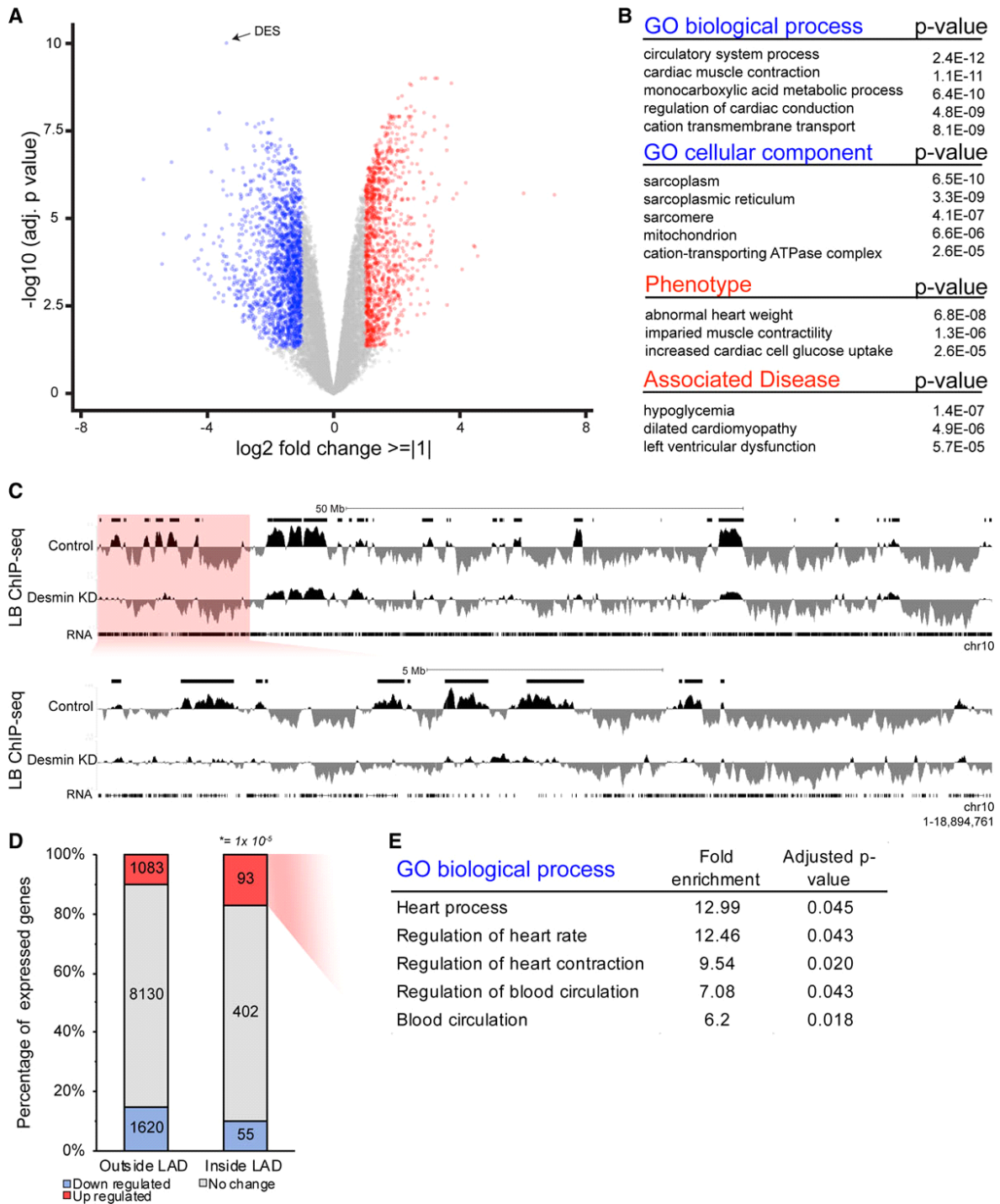
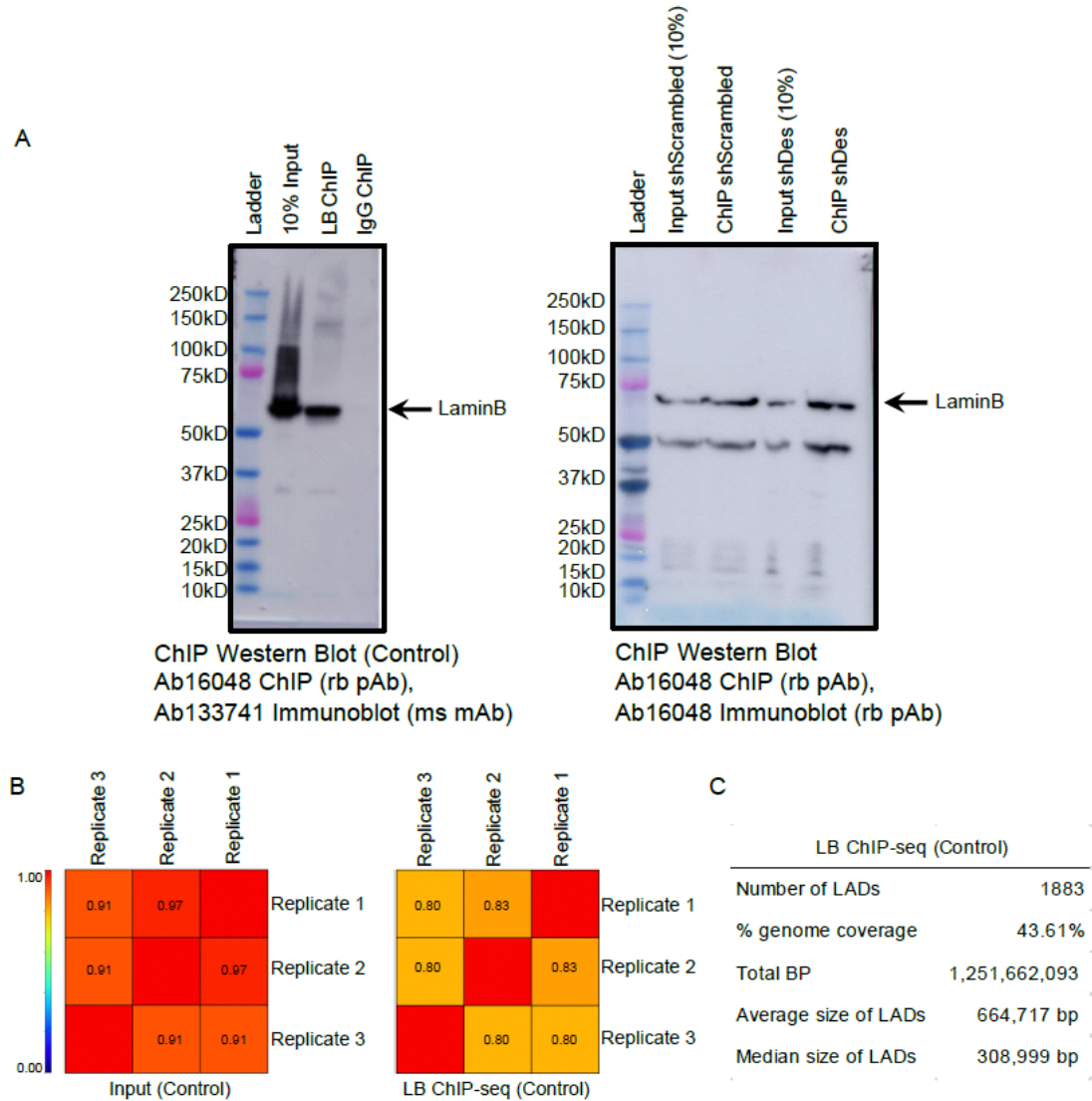


Figure 9: Desmin knockdown (KD) results in large-scale changes to gene expression and compromises lamina-bound chromatin.

A, RNAseq was performed on scramble/null and desmin KD cardiomyocytes. Volcano plot showing differentially expressed genes on desmin depletion compared with scramble. Genes were considered significantly different with a log2 fold

change $\geq |1|$ and false discovery rate of 0.05. Red indicates upregulated transcripts, while blue indicates downregulated transcripts. **B**, Gene Ontology (GO) Analysis of differentially expressed genes via TopGene, showing the most significantly altered groups of genes on desmin depletion, as well as associated phenotypes or diseases associated with the desmin KD transcriptome (blue and red titles do not indicate directionality of gene expression). **C**, Representative lamin B chromatin immunoprecipitation (ChIP)-seq track from entire chromosome 10 (rn6). Lamina-associated domains (LADs) are labeled with black boxes immediately above track. Area in red box is magnified in bottom track (1–18 894 761 bp of chromosome 10). **D**, Stacked bar chart indicating percentage of genes which changed expression on desmin KD (\log_2 fold change $\geq |1|$ and adjusted $P < 0.05$), categorized as whether they resided inside or outside a LAD in control conditions. Number of genes indicated in bar chart. The distribution of upregulated and downregulated genes in and out of LADs is significantly different as determined via χ^2 comparison (χ^2 statistic = 32.2). **E**, PantherDB GO analysis of the 93 genes which resided in LADs in control cells and were upregulated on desmin depletion.



Supplemental Figure 6: Lamin-B1 ChIP immunoprecipitation (IP) and sequencing are both functional. **A**, LaminB1 ChIP-western in indicated conditions. **B**, Spearman correlation coefficients comparing occupancy between replicates of either input or LB ChIP-seq from control samples on chr1. **C**, Indicated statistics upon merging three replicates and then identifying EPIC-based lamin-associated domains (LADs) from control sample.

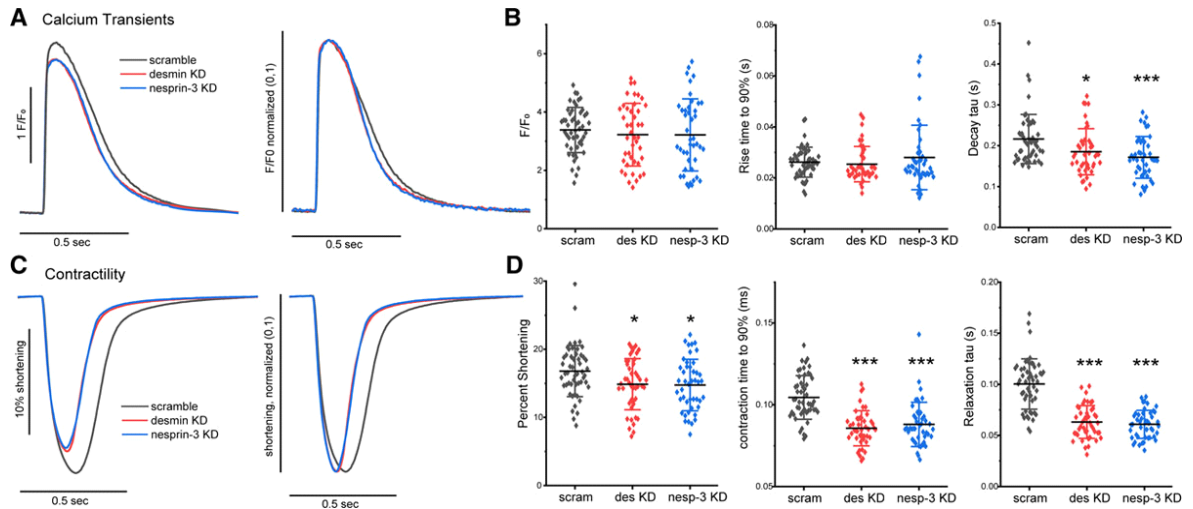


Figure 10: Excitation-contraction coupling is similarly altered upon acute desmin or nesprin (nuclear envelope spectrin repeat protein)-3 depletion. A, Left, change in cytosolic calcium (F/F_0) and right, amplitude-normalized F/F_0 time course of Fluo-3 loaded adult rat cardiomyocytes electrically stimulated at 1 Hz. **B, Quantification of $[Ca^{2+}]_i$ transient amplitude (left), rise time (middle), and decay τ (right).** Scramble: N=3, n=52 cells. Desmin knockdown (KD): N=3, n=45 cells. Nesprin-3 KD: N=3, n=45 cells. **C, Left,** average contractility trace (sarcomere shortening) and right, amplitude-normalized shortening of the identical adult rat cardiomyocytes from experiment in A. **D, Quantification of contractile amplitudes (left) shortening time (middle) and relaxation τ (right).** Statistical significance determined via 1-way ANOVA with Bonferroni correction. For statistical significance, * $P < 0.05$, ** $P < 0.01$, *** $P < 0.001$ vs control.

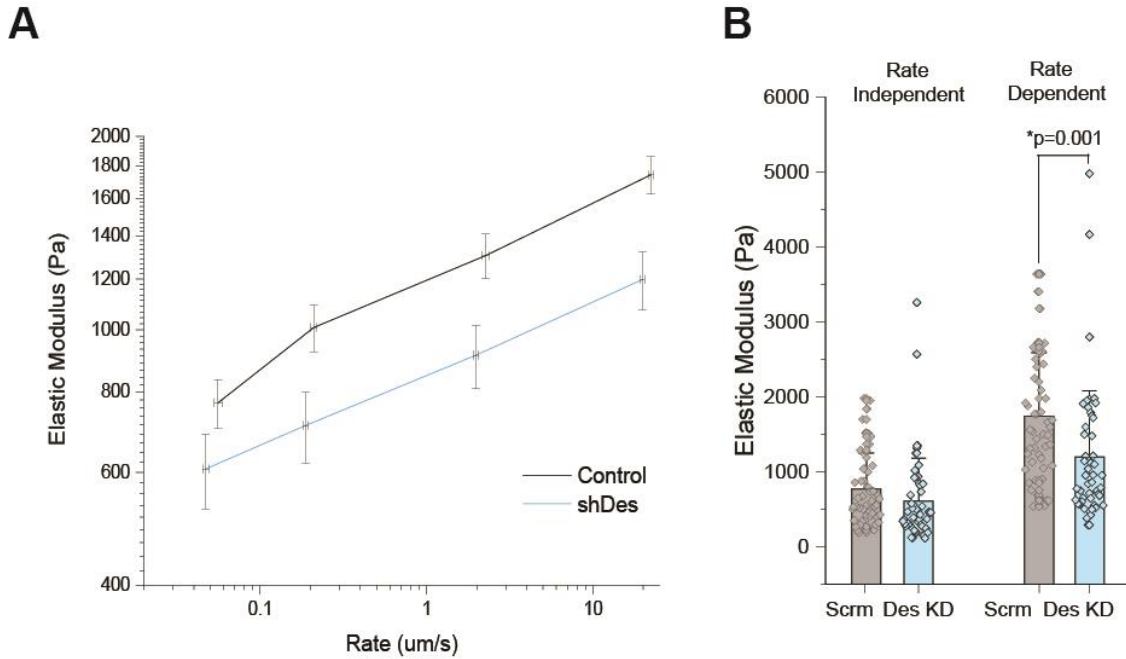


Figure 11: Desmin KD decreases the viscoelasticity of adult cardiomyocytes. **Left**, the elastic modulus (Pa) measured over different indentation rates. Des KD/shDes shows a trend in a decreasing stiffness over all indentation rates. **Right**, however, Des KD shows a significantly lower stiffness at the highest indentation rates. These data suggest that desmin KD preferentially decreases viscoelasticity over elastic behavior. Control: N= 5 rats, n= 52 cells. Des KD: N= 5, n= 51. P value shown indicates vs rate-dependent control. Statistical analysis was performed by doing a two-way ANOVA with Bonferroni correction.

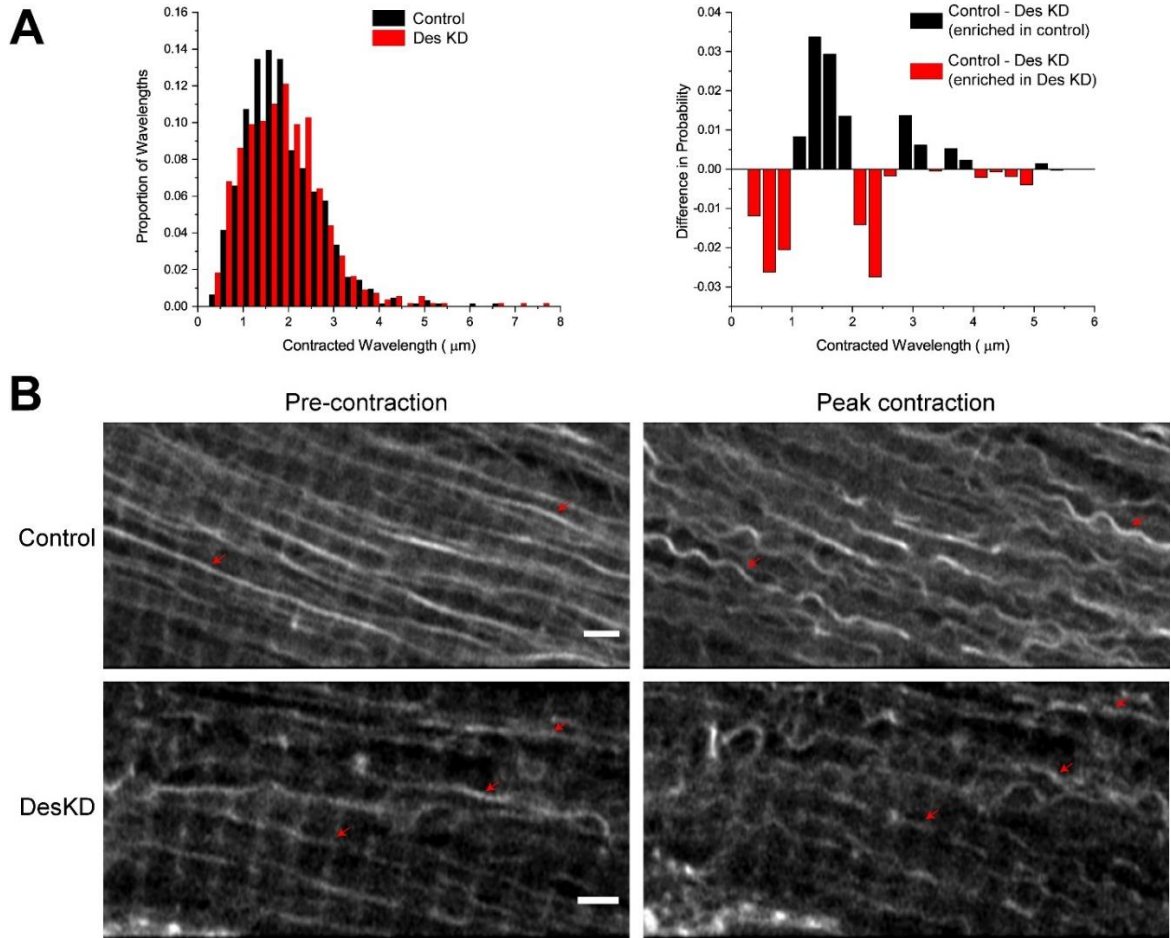


Figure 12: Desmin KD causes microtubules to contract with longer wavelengths. A, Left, Proportion of buckles measured showing a right-ward shift in the distribution in response to desmin KD. This is significant because the adult rat cardiomyocyte tends to contract to 1.5-1.7 μm . This is also the observed wavelength of normal microtubule buckles as shown by the black distribution. The right-ward shift indicates a loss of rigid attachment of microtubules to the z-disc. **Right,** the same data but presented as a difference in proportion to highlight the change in distributions at 1 (1.5 μm) or 2 (3 μm) contracted sarcomere lengths. Control, contracted: N= 5 rats, n= 624 wavelengths. Des KD, contracted: N= 5, n=544. **B,** Representative images of microtubule buckling with either control or desmin KD. Small red arrows have been added to allow readers to easily track the same microtubule between images.

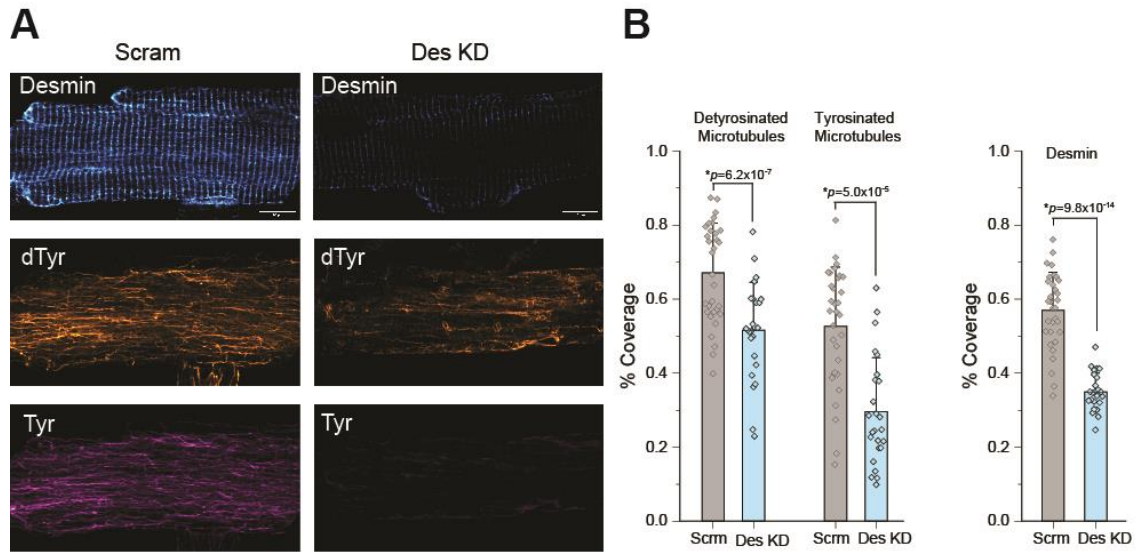


Figure 13: Desmin KD reduces tyrosinated microtubules. **A**, Representative images showing the decrease in desmin (cyan), detyrosinated (dTyr, orange) and tyrosinated (Tyr, magenta) microtubules in adult rat cardiomyocytes with desmin KD. **B**, Quantification of the percent cell coverage of dTyr, Tyr (**left**) and desmin (**right**). Scram: N= 2 rats, n= 32 cells. Des KD: N= 2, n= 25. Statistical analysis was performed using two-sample t-test.